# The Ca and Mg isotope record of the Cryogenian Trezona carbon isotope excursion

Anne-Sofie C. Ahm[a,*], Christian J. Bjerrum[b], Paul F. Hoffman[c], Francis A. Macdonald[d], Adam C. Maloof[a], Catherine V. Rose[e], Justin V. Strauss[f], John A. Higgins[a]

[a] *Princeton University, Guyot Hall, Princeton, NJ 08540, USA*
[b] *University of Copenhagen, Øster Voldgade 10, 1350 Copenhagen K, Denmark*
[c] *University of Victoria, School of Earth and Ocean Sciences, BC, Canada*
[d] *University of California, Santa Barbara, Department of Earth Science, CA 93106*
[e] *University of St Andrews, Irvine Building, St. Andrews, United Kingdom*
[f] *Dartmouth College, Fairchild Hall, Hanover, NH 03755, USA*

---

---



*Please address correspondence to
*Email address:* aahm@princeton.edu (Anne-Sofie C. Ahm)

**Abstract:** The Trezona carbon isotope excursion is recorded on five different continents in platform carbonates deposited prior to the end-Cryogenian Marinoan glaciation (>635 Ma) and represents a change in carbon isotope values of 16–18‰. Based on the spatial and temporal reproducibility, the excursion previously has been interpreted as tracking the carbon isotopic composition of dissolved inorganic carbon in the global ocean before the descent into a snowball Earth. However, in modern restricted shallow marine and freshwater settings, carbon isotope values have a similarly large range, which is mostly independent from open ocean chemistry and instead reflects local processes. In this study, we combine calcium, magnesium, and strontium isotope geochemistry with a numerical model of carbonate diagenesis to disentangle the degree to which the Trezona excursion reflects changes in global seawater chemistry versus local shallow-water platform environments. Our analysis demonstrates that the most extreme carbon isotope values (∼-10‰ versus +10‰) are preserved in former platform aragonite that was neomorphosed to calcite during sediment-buffered conditions and record the primary carbon isotope composition of platform-top surface waters. In contrast, the downturn and recovery of the Trezona excursion are recorded in carbonates that were altered during early fluid-buffered diagenesis and commonly are dolomitized. We also find that the nadir of the Trezona excursion is associated with a fractional increase in siliciclastic sediments, whereas the recovery from the excursion correlates with a relative increase in carbonate. This relationship suggests that the extreme negative isotopic shift in platform aragonite occurred in concert with periods of increased input of siliciclastic sediments, changes in water depth, and possibly nutrients to platform envi-

ronments. Although the process for generating extremely negative carbon isotope values in Neoproterozoic platform carbonates remains enigmatic, we speculate that these excursions reflect kinetic isotope effects associated with $CO_2$ invasion in platform waters during periods of intense primary productivity.

## 1. Introduction

The Cryogenian Period (∼720–635 Ma) of the Neoproterozoic Era is characterized by major reorganizations of Earth surface processes and is bracketed by two Snowball Earth events, the older Sturtian and the younger Marinoan glaciation (Hoffman et al., 1998). However, many important aspects of these evolutionary and climatic changes remain enigmatic due to the sparsity of radiometric age constraints and the challenges of interpreting geochemical records from ancient platform carbonates.

To overcome the lack of both radiometric age constraints and biostratigraphy in Neoproterozoic successions, $\delta^{13}C$ stratigraphy has been used as a global correlation tool. Cryogenian carbonates are characterized by significant variability in the isotopic ratios of $^{13}C/^{12}C$ ($\delta^{13}C$), with excursions of similar shape and magnitude recorded in multiple locations (Halverson et al., 2005). The reproducibility of $\delta^{13}C$ excursions across continents is broadly supported by strontium isotopes ($^{87}Sr/^{86}Sr$) and radiometric ages (Fig. 1), which has served as evidence that these excursions directly record perturbations in the global carbon cycle (e.g., Kaufman et al., 1997; Hoffman and Schrag, 2002). However, the interpretation that $\delta^{13}C$ in Neoproterozoic platform carbonates records the isotopic composition of dissolved inorganic

carbon (DIC) of open-ocean seawater is at odds with observations from modern to Miocene platform and periplatform carbonates. In contrast to pelagic sediments deposited in the deep sea, carbonates that originally precipitated on shallow banks often do not reflect the average carbonate sink (Swart and Eberli, 2005; Swart, 2008).

Over geological time scales, the net input of carbon to the atmosphere must be balanced by the burial of organic matter and carbonate sediment, with bulk carbonate $\delta^{13}$C values controlled by the fraction of organic matter burial globally ($f_{org}$, e.g., Kaufman et al., 1997). However, $\delta^{13}$C values of platform-derived carbonate are sensitive to restriction of marine circulation, primary productivity (Patterson and Walter, 1994; Geyman and Maloof, 2019), and early diagenetic alteration driven by the advection of both seawater and meteoric water within the sediment pile (Allan and Matthews, 1982; Melim et al., 2002). During time periods where carbonate burial is concentrated in platform environments, the impact of widespread local changes of depositional environments on global mass balance needs to be reevaluated (Geyman and Maloof, 2019). As a major constituent in carbonate ($CaCO_3$), calcium isotope ratios ($\delta^{44/40}$Ca) provide an independent constraint on the average carbonate sink. The main sink for seawater $Ca^{2+}$ is the burial of carbonate sediments and a prediction for the global calcium cycle is that, on average, the isotope composition of carbonate through time should equal that of Bulk Silicate Earth (BSE = -1‰, Skulan et al., 1997; Blättler and Higgins, 2017). In other words, what comes in must go out, and if sampling the average carbonate sink, $\delta^{44/40}$Ca values should approach ∼-1‰ when averaged over thick carbonate successions. As a result, $\delta^{44/40}$Ca values pro-

vide a tool to reconcile the decoupling between platform environments and the global ocean, the requirements of global mass balance, and the lack of absolute time constraints from individual Neoproterozoic successions.

In this study, we investigate the variability of carbonate $\delta^{44/40}$Ca values across the Trezona excursion, a large negative $\delta^{13}$C excursion recorded on multiple continents prior to the Marinoan glaciation. This $\delta^{13}$C excursion reaches values of $\sim -10‰$ and occurs stratigraphically above a prolonged interval with mostly high $\delta^{13}$C values (up to $+10‰$, Kaufman et al., 1997; Halverson et al., 2005). The timing of the excursion is broadly constrained to within the Cryogenian 'non-glacial' interlude (between 660 and 640 Ma, Fig. 1). By combining measurements of $\delta^{44/40}$Ca with Mg isotopes ($\delta^{26}$Mg), $^{87}$Sr/$^{86}$Sr, and Sr/Ca and Mg/Ca ratios in bulk carbonate from multiple sections in Australia, Namibia, and Canada, we test to what extent the Trezona $\delta^{13}$C excursion has been altered by diagenesis. We use the geochemical data to fingerprint samples that have preserved their primary $\delta^{13}$C values during sediment-buffered diagenesis in contrast to $\delta^{13}$C values that have been reset during fluid-buffered diagenesis. We find that intervals characterized by fluid-buffered diagenesis have less extreme $\delta^{13}$C values, and $\delta^{44/40}$Ca closer to BSE, relative to intervals characterized by sediment-buffered diagenesis. These results demonstrate that the most extreme $\delta^{13}$C values, both positive and negative, are primary in origin and are associated with local controls on $\delta^{13}$C in shallow-water aragonite producing environments.

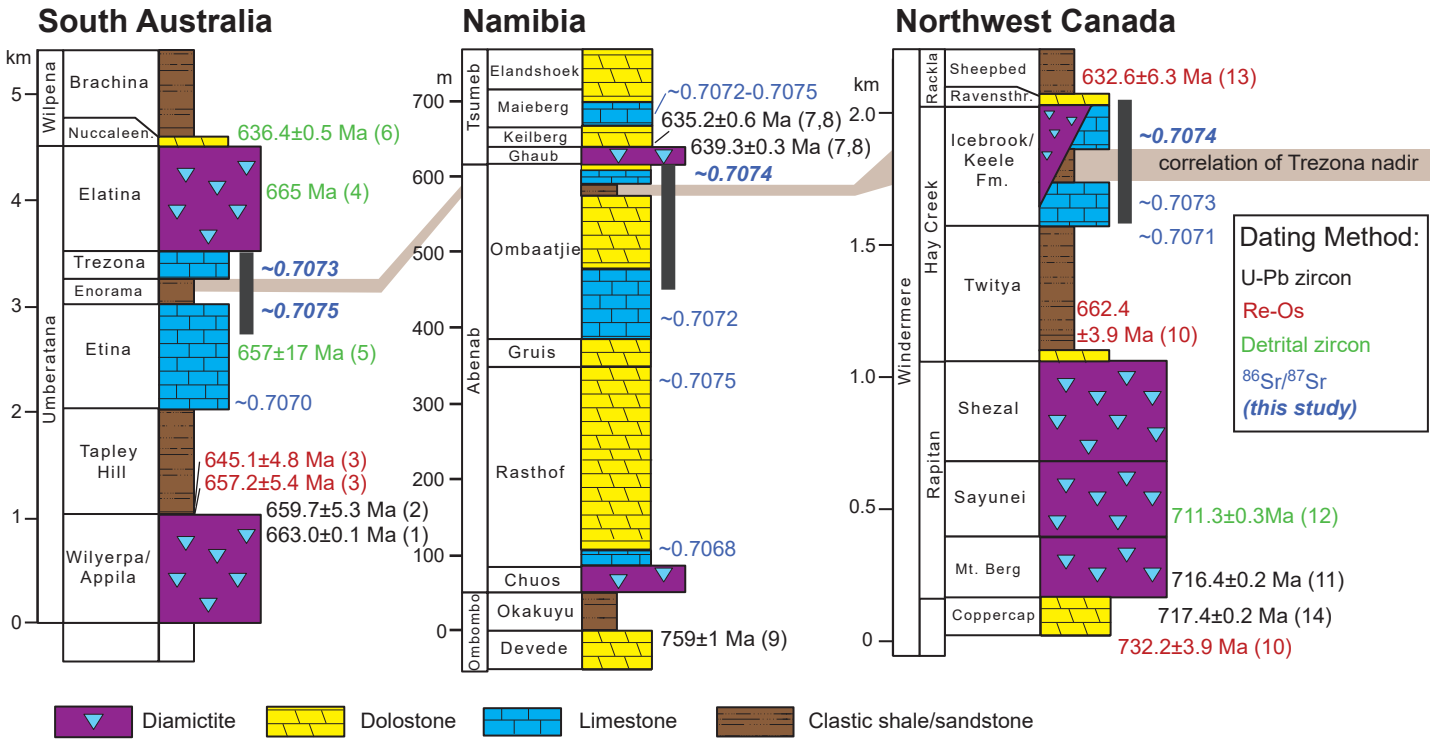


Figure 1: Generalized Cryogenian strata from South Australia, Namibia, and Northwest Canada. Note changes in scale. Dark gray bars indicate the stratigraphic intervals studied here. All successions are characterized by two glacial horizons – the lower Sturtian and the upper Marinoan glaciation – which have been correlated by radiometric dates. However, carbonates deposited during the non-glacial interlude have few radiometric age constraints and have been correlated based on carbon and strontium isotope stratigraphy (published $^{87}Sr/^{86}Sr$ ratios from Halverson et al., 2005, 2007). Dates from South Australia are from: (1) Cox et al. (2018), (2) Fanning and Link (2008), (3) Kendall et al. (2006), (4) Rose et al. (2013), (5) Preiss (2000), (6) Calver et al. (2013). Dates from Namibia are from: (7) Prave et al. (2016), (8) Hoffmann et al. (2004), (9) Halverson et al. (2005). Dates from Northwest Canada are from: (10) Rooney et al. (2014), (11) Macdonald et al. (2010), (12) Baldwin et al. (2016), (13) Rooney et al. (2015), (14) Macdonald et al. (2018)

## 2. Methods

### *2.1. Stratigraphical sections*

In this study, we investigate the geochemical variability of three different Cryogenian carbonate successions (12 stratigraphic sections), from South Australia, Namibia, and Northwest Canada. At each locality, the sedimentology and $\delta^{13}$C chemostratigraphy has been extensively studied in previous publications (e.g., McKirdy et al., 2001; Rose et al., 2012; Klaebe and Kennedy, 2019; Hoffman, 2011; Macdonald et al., 2018), and we refer to the supplementary material for a detailed summary of the geological setting with location maps (Fig. S1–S3). For each locality, the stratigraphy and radiometric age constraints are summarized in Fig. 1.

### *2.2. Geochemical analyses*

All measurements presented in this study are performed on carbonate powders that previously have been measured for $\delta^{13}$C and $\delta^{18}$O values (Strauss et al., unpublished; Hoffman, 2011; Rose et al., 2012, 2013; Macdonald et al., 2018). We refer to the supplementary material for a detailed outline of the Ca, Mg, and Sr isotope analyses and major and trace element analyses.

Calcium isotope measurements are reported for all samples as the relative abundance of $^{44}$Ca relative to $^{40}$Ca using standard delta notation, normalized to the isotopic composition of modern seawater. For Ca isotopes, the external reproducibility for SRM915b and SRM915a relative to modern seawater is $-1.19 \pm 0.14$‰ ($2\sigma, N = 120$) and $-1.86 \pm 0.16$‰ ($2\sigma, N = 24$), respectively.

Magnesium isotope ratios are reported as the relative abundance of $^{26}$Mg versus $^{24}$Mg, normalized to DSM-3. For Mg, the long-term external reproducibility for Cambridge-1 and seawater are $-2.61 \pm 0.10$‰ ($2\sigma, N = 81$)

and $-0.83 \pm 0.11‰$ ($2\sigma, N = 47$), respectively.

A subset of samples was selected for strontium isotope analyses, performed at both Princeton University (samples from Namibia and Australia) and WHOI (samples from Northwest Canada). Strontium isotope measurements are reported as the ratio of $^{87}$Sr over $^{86}$Sr. At Princeton University, the long-term reproducibility of NBS987 is $0.710280 \pm 0.000006$ ($N = 4$). At WHOI, the long-term reproducibility of NBS987 is $0.710253 \pm 0.000015$ ($N = 12$). To reduce the influence of in-situ Rb decay ($^{87}$Rb to $^{87}$Sr), measurements were filtered for Sr/Ca ratios >1.5 mmol/mol and reported as the average filtered value for each section, consistent with methods from previous publications (Halverson et al., 2005). In section F1228, where Sr/Ca ratios are low, $^{87}$Sr/$^{86}$Sr ratios instead were filtered based on the least radiogenic values.

### *2.3. Numerical Diagenetic Model*

To analyze the geochemical data, we use a numerical model of early carbonate diagenesis. This model previously has been used to simulate diagenetic changes in both Bahamian and Neoproterozoic carbonate (Ahm et al., 2018, 2019; Bold et al., 2020; Crockford et al., 2020).

The model computes the geochemical changes that occur during early diagenesis as metastable carbonate minerals (e.g., aragonite) are dissolved and more stable phases (e.g., dolomite) precipitate. The conceptual model framework is a simplification of the complex geometry of fluid flow and diagenesis in carbonate sediments, which is affected by local differences in porosity, permeability, and reaction rates. To account for these differences, we present the model results as 2-dimensional phase-spaces (Fig. 2). These

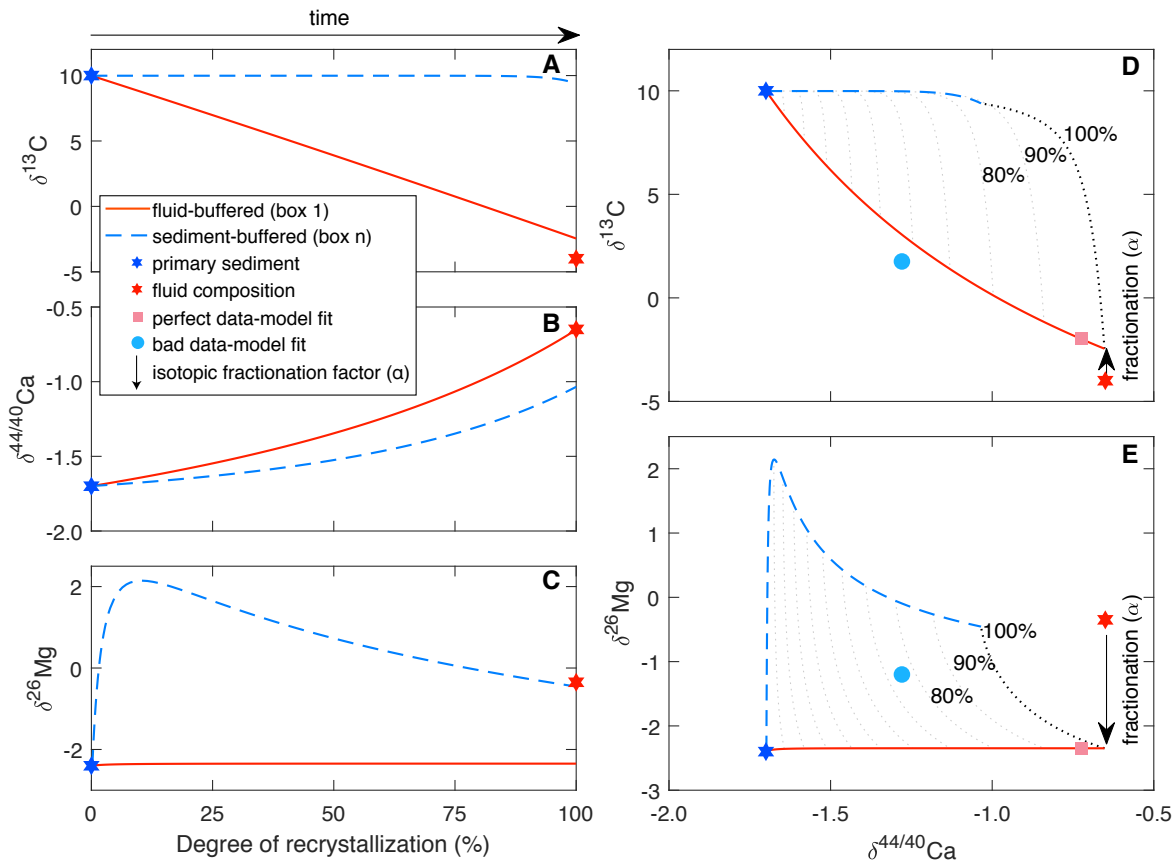


Figure 2: Numerical diagenetic model demonstrating the change in bulk carbonate chemistry over time with increasing degree of alteration, in this case modeled as dolomitization (from 0-100%), in both fluid- (box 1, blue dashed line) and sediment-buffered (box n, red solid line) conditions (following methods outlined by Ahm et al., 2018). **A.** The change in carbonate $\delta^{13}$C values over time from a primary value of 10‰ (blue star) towards a fluid value of -4‰ (red star), accounting for a fractionation factor of +1‰ between pore-fluid and the diagenetic carbonate minerals (Table S1). **B.** The change in carbonate $\delta^{44/40}$Ca values from a primary value of -1.7‰ towards a fluid value of -0.65‰, with a fractionation factor of 0‰ (Fantle and DePaolo, 2007; Jacobson and Holmden, 2008). **C.** The change in carbonate $\delta^{26}$Mg values from a primary value of -2.4‰ towards a fluid value of -0.35‰, with a fractionation factor of -2‰ (Higgins and Schrag, 2010). As the rate of dolomitization decrease with time, the inflection in the sediment-buffered $\delta^{26}$Mg pathway represents the point where the supply of new $Mg^{2+}$ from advection overcomes the decrease of $Mg^{2+}$ due to dolomitization. **D.** Cross-plot of $\delta^{13}$C versus $\delta^{44/40}$Ca using the model outputs from A and B. **E.** Cross-plot of $\delta^{26}$Mg versus $\delta^{44/40}$Ca using the model outputs from B and C. Note that the model phase space in D and E are insensitive to changes in both reaction and advection rate, as changes in either of these parameter would have a similar impact on both the y and x-axis. The model is fit to the data using the phase space in D and E, where the goodness of fit is evaluated in part by the consistency of the model to predict a similar degree of alteration (%) for the same sample. A good model fit (pink square) is indicated by a similar degree of alteration across the phase spaces, whereas a bad fit (blue circle) is indicated by an offset in the predicted degree of alteration across the phase spaces and being outside the phase space in D.

model cross-plots represent the geochemical changes that occur at different stages of diagenetic alteration (from 0-100%) and fluid evolution along the flow path (fluid- to sediment-buffered). In other words, each cross-plot comprises the total geochemical variability that can be produced from reactions between a carbonate rock and a diagenetic fluid with a prescribed composition.

We use the model results to evaluate to what degree the geochemical signals across the Trezona excursion are products of diagenesis. By fitting the model phase space to envelope the data, we can estimate the composition of diagenetic fluids and different primary sedimentary end-members (Fig. 2D-E). We refer to the supplementary material for a detailed description of the model setup and evaluation of specific model fits using a bootstrap resampling technique.

## 3. Results

### *3.1. South Australia*

In South Australia, the upper part of the Cryogenian succession contains the Trezona excursion (McKirdy et al., 2001; Rose et al., 2012). Stratigraphically below the excursion, the shallow-water limestone of the Etina Formation is characterized by high $\delta^{13}$C values ∼+10‰, relatively constant $\delta^{44/40}$Ca values ranging between -1.6 and -1.2‰, and Sr/Ca ratios that average 0.86 mmol/mol (ranging between 0.12–2.2 mmol/mol, Fig. 3A-B). The most Sr-rich samples have $^{87}$Sr/$^{86}$Sr ratios between ∼0.7075–0.708.

The downturn of the Trezona excursion is not observed, due to a lack of carbonate in the Enorama Shale (Fig. 1). The nadir of the excursion is recorded in the lower part of the Trezona Formation, characterized by a high

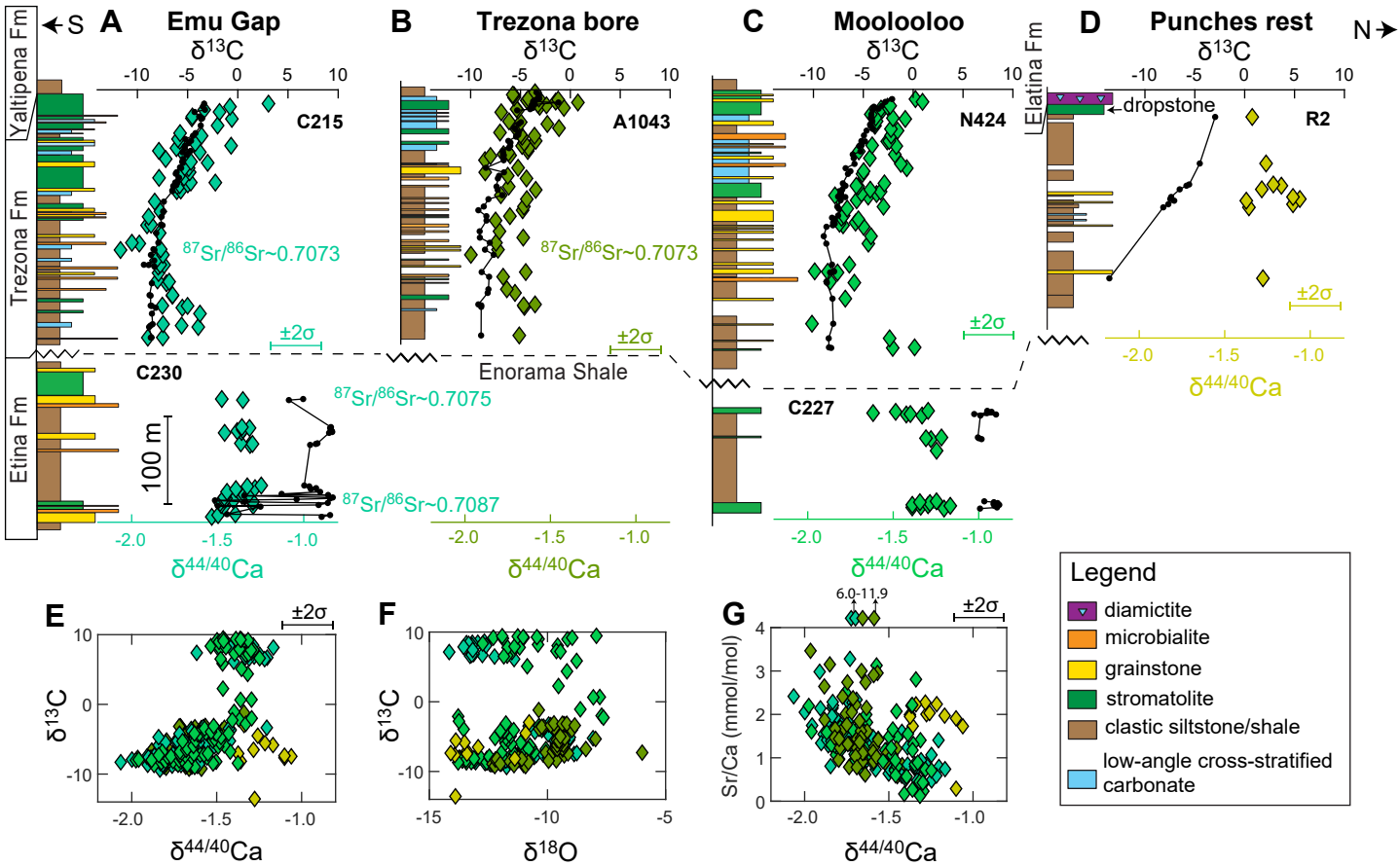


Figure 3: **South Australia:** The Trezona Formation is correlated across the basin based on carbon isotopes and the stratigraphic position of the Enorama Shale below and the glacigenic Elatina Formation above (Rose et al., 2012, 2013). Sections C215, N424, and A1043 are from the Central Flinders Ranges, while section R2 is from the Northern Flinders Ranges (for location map see Fig. S1).

fraction of fine-grained siliciclastic material relative to carbonate, with $\delta^{13}$C values at ∼-10‰ (McKirdy et al., 2001; Rose et al., 2012). Generally, this interval also records low $\delta^{44/40}$Ca values down to ∼-2‰ , low $\delta^{18}$O values (down to -15‰), and high Sr/Ca ratios averaging ∼1.7 mmol/mol. The most Sr-rich samples have $^{87}$Sr/$^{86}$Sr ratios of ∼0.7073.

The recovery of the excursion spans ∼250 m, with a gradual return to higher $\delta^{13}$C values approaching ∼0‰ at the top of the succession. This interval also records broadly increasing $\delta^{18}$O values (towards -8‰), increasing $\delta^{44/40}$Ca values up to -1.2‰, and decreasing Sr/Ca ratios (Fig. 3). While the depositional environment in the nadir of the excursion is characterized by siliciclastic sediments, the increase in $\delta^{13}$C values up section coincides with a broad increase in relative carbonate abundance (McKirdy et al., 2001; Rose et al., 2012). This coarsening upwards succession previously has been interpreted as representing a shallowing (McKirdy et al., 2001; Rose et al., 2013), but this interpretation recently has been challenged (Klaebe and Kennedy, 2019).

### *3.2. Namibia*

Namibia is the only location that has a progressive record of the Trezona excursion downturn (Fig. 4). The Trezona excursion is found in the upper Ombaatjie Formation and records a steady decline in $\delta^{13}$C values down from ∼+7 to -7‰ over a stratigraphic interval of 40–80 m. This interval also records decreasing $\delta^{44/40}$Ca values (from -0.7 to -1.6‰), decreasing $\delta^{18}$O values (from -1 to -8‰), and increasing $\delta^{26}$Mg values (from -2.1 to -1.0‰). However, the changes in $\delta^{44/40}$Ca, $\delta^{18}$O, and $\delta^{26}$Mg values begin stratigraphically after the downturn of the $\delta^{13}$C excursion has reached 0‰ (Fig. 4B-C).

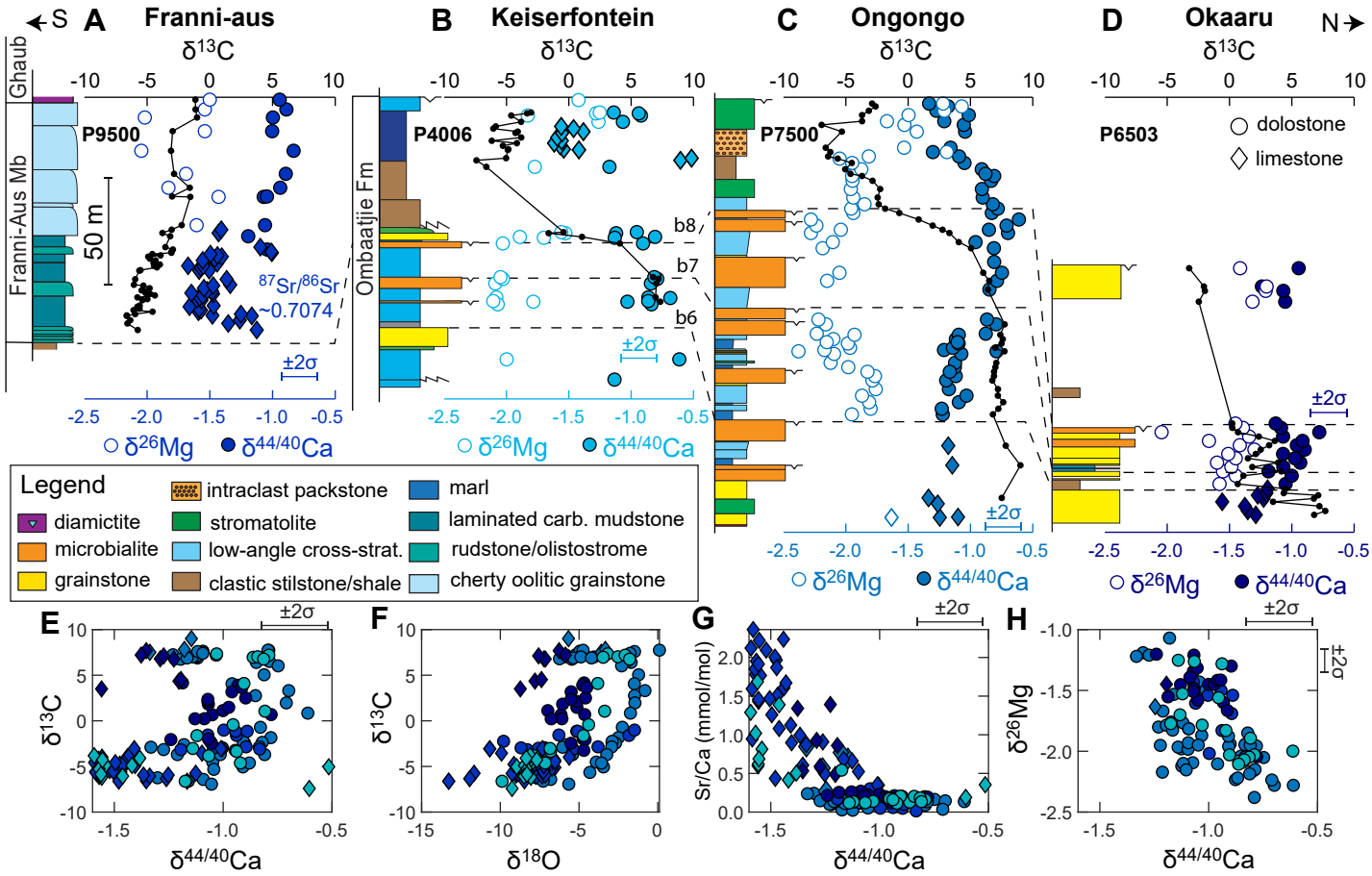


Figure 4: **Namibia:** Section P4006, P7500, and P6503 are shallow-water carbonates from the Ombaatjie Formation that record the downturn of the Trezona excursion. Section P9500 is from the more distal Franni-aus Member and only records the recovery of the Trezona excursion. The nadir of the Trezona excursion conincides with deposition of a regional siltstone unit with varying thickness, termed the Narachaams Member on the foreslope. The platform sections are correlated (dashed lines) based on observed parasequences (previously termed b4-b8), while the foreslope section (P9500) is related to the platform using $\delta^{13}$C chemostratigraphy Hoffman for location map see Fig S2, 2011).

While the downturn of the excursion is hosted in the shallow-water dolostone of the Ombaatjie platform, the nadir of the excursion coincides with a change from carbonate to a unique fine-grained siliciclastic unit (parasequence b8, Hoffman, 2011). The Ombaatjie platform has a well-defined southern limit, beyond which is a foreslope with redeposited carbonates (Hoffman, 2011). On the foreslope, the siliciclastic siltstone unit (the Narachaams Member) is thicker (>100 m) than on the platform, and the downturn of the Trezona excursion is not recorded. Above the siltstone, carbonate deposition returns in the form of a 100-m-thick coarsening upward succession (Franniaus Member) that records the nadir and a somewhat more complete recovery from the Trezona excursion than is preserved on the platform (from -7 towards 0‰). In parallel, this interval also records increasing $\delta^{18}$O values (from -13 to -2‰), increasing $\delta^{44/40}$Ca values (from ∼-1.6 to -0.8‰), decreasing Sr/Ca ratios, and $\delta^{26}$Mg values between -2 and -1.5‰ (Fig. 4). The Sr-rich limestone preserving $^{87}$Sr/$^{86}$Sr ratios of ∼0.7074.

### *3.3. Northwest Canada*

In the Mackenzie Mountains (sections J1132/33), the Trezona excursion is recorded in the upper Keele Formation. Stratigraphically below the excursion, the shallow-water carbonate of the lower Keele Formation is characterized by a plateau of high $\delta^{13}$C values (the 'Keele peak', ∼+10‰, Kaufman et al., 1997; Day et al., 2004). The limestone and dolostone found in this interval have $\delta^{44/40}$Ca values between -1.2 and -1.0‰, high $\delta^{26}$Mg values up to ∼-0.6‰, and Sr/Ca ratios averaging 0.7 mmol/mol (Fig. 5). The more Sr-rich samples has $^{87}$Sr/$^{86}$Sr values of ∼0.7073.

The carbonates containing the 'Keele peak' are succeeded by siliciclastic

dominated strata (the 'Keele clastic wedge', Aitken, 1991; Day et al., 2004). Overlying the Keele clastic wedge, the Trezona nadir is found within subtidal limestone and contains $\delta^{13}$C values down to -10‰, $\delta^{44/40}$Ca values down to -1.9‰, Sr/Ca values up to 4 mmol/mol, and $^{87}$Sr/$^{86}$Sr ratios of ∼0.7074 (Fig. 5). Following the nadir of the excursion, the uppermost stata of the Keele Formation record increasing $\delta^{13}$C values before the deposition of glacial sediments. Across this interval, $\delta^{44/40}$Ca values increase towards -1‰ and Sr/Ca ratios decrease to <1 mmol/mol.

In the Wernecke Mountains, the Trezona excursion is recorded in the Durkan Member of the Ice Brook Formation. Stratigraphically below the Durkan Member, is the Mount Profeit dolostone recording $\delta^{13}$C values between ∼0 to +5‰ (Macdonald et al., 2018). This interval has $\delta^{44/40}$Ca values between ∼-1.5 and -1‰, $\delta^{18}$O values between ∼-11 to -8‰, and Sr/Ca ratios between 0.6 and 1.5 mmol/mol. Samples with low $\delta^{44/40}$Ca and high Sr/Ca ratios record $^{87}$Sr/$^{86}$Sr ratios of ∼0.7073–0.7076.

The Durkan Member consists of siltstone and shale with thin-bedded limestone and multiple horizons of carbonate clast breccia (section F1228, Macdonald et al., 2018). This interval contains the nadir and recovery of the Trezona excursion, recording values that increase from -10‰ towards 0‰ across ∼250 m. The recovery of the excursion coincides with an increase in carbonate deposition relative to siliciclastics and an increase in $\delta^{44/40}$Ca values from -1.8 to -1.0‰. This interval also records high Sr/Ca ratios up to 2.5 mmol/mol, and relatively scattered $\delta^{18}$O values (from -6 to -12‰, Fig. 5).

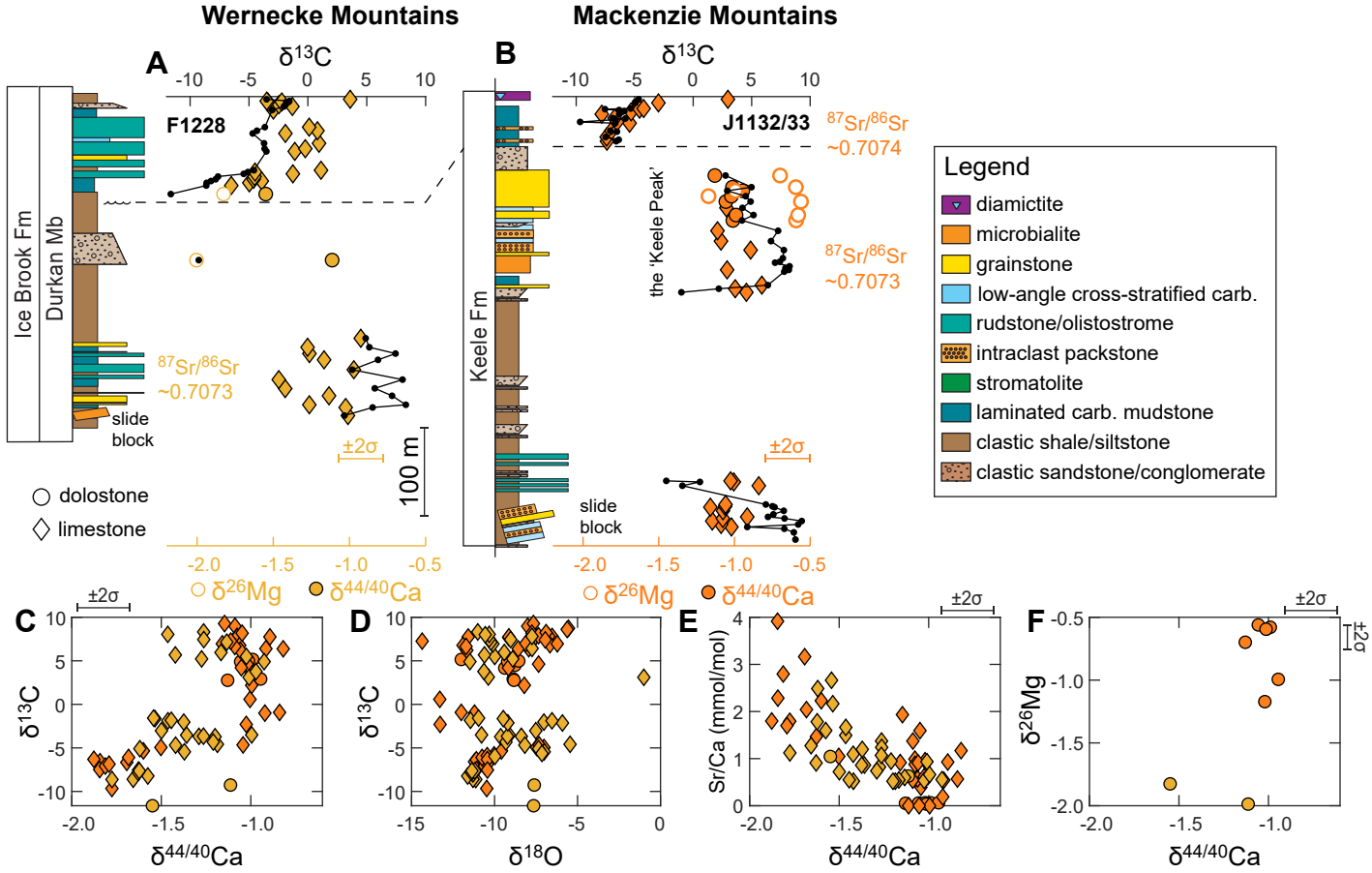


Figure 5: **Northwest Canada:** Stratigraphic columns and isotopic measurements from Northwest Canada. Section F1228 is from the Wernecke Mountains in Yukon while sections J1132 and J1133 are from the Mackenzie Mountains in the Northwest Territories (for location maps see Fig. S3).

## 4. Discussion

### *4.1. The Trezona excursion – global and local controls*

Despite the fact that the Trezona downturn is followed by sometimes hundreds of meters of $\delta^{13}$C recovery towards 0‰, previous models have focused on interpreting the decline in $\delta^{13}$C as associated with global changes in sea water chemistry and the onset of Snowball Earth (e.g., Hoffman and Schrag, 2002; Tziperman et al., 2011). Here, however, we highlight three features of the relationship between carbon and calcium isotopes across the entire Trezona excursion that are inconsistent with this interpretation.

First, we consider to what degree the $\delta^{44/40}$Ca values that are observed across the Trezona excursion may reflect steady state changes in the global calcium cycle. The main sink for seawater $Ca^{2+}$ is the burial of carbonate. A prediction for the global calcium cycle is that, on average, the calcium isotope composition of carbonate sediments through time should equal that of BSE ($\sim -1$‰, on time-scales $>10^6$ years, Skulan et al., 1997; Blättler and Higgins, 2017). However, the majority of the Cryogenian samples have $\delta^{44/40}$Ca <-1‰ (Fig. 6), both before the Trezona excursion and in the Trezona nadir, and mass balance requires that these sediments cannot represent the average carbonate sink over long time scales.

Second, we consider to what degree the synchronicity of the carbon and calcium isotope excursions are consistent with a transient change in global carbonate burial. On the surface of Earth, the residence time for calcium is an order of magnitude longer than for carbon ($\sim 10^6$ versus $\sim 10^5$ years, e.g., Gussone et al., 2020). Therefore, any perturbation to carbonate burial should not result in a synchronous stratigraphic change in carbonate $\delta^{13}$C

and $\delta^{44/40}$Ca values, if we assume that the relative residence time of the calcium and carbon cycles were scaled similarly to today, (Holmden et al., 2012b). If the Trezona excursion represents a transient perturbation, the $\delta^{44/40}$Ca excursion should take longer to recover than the $\delta^{13}$C excursion. However, the Trezona data records covariation with no lag between carbon and calcium isotopes (Fig. 3–5).

Third, we consider to what degree the magnitude of the Trezona $\delta^{44/40}$Ca downturn and recovery is consistent with a transient perturbation in global seawater (<1 Myrs). There are three main mechanisms that can cause a negative calcium isotope excursion: (1) increased weathering, (2) ocean acidification, or (3) a change from calcite to aragonite seas (e.g., Gussone et al., 2020). Numerical models that include the coupled calcium-carbon cycle, and the inherent links to carbonate saturation and precipitation rates, have demonstrated that the maximum $\delta^{44/40}$Ca excursion that can occur from the combined effects of increased weathering and ocean acidification is $\sim -0.3$‰ (Komar and Zeebe, 2016). In addition, a switch in the dominant mineralogy of the average carbonate sink from calcite to aragonite could cause a transient negative excursion in carbonate $\delta^{44/40}$Ca values, as aragonite is -0.5‰ more depleted in $^{44}$Ca than calcite (Gussone et al., 2005). In this scenario, once a new steady state is reached (<1 myrs after), seawater $\delta^{44/40}$Ca will be 0.5‰ higher and $\delta^{44/40}$Ca values of the average carbonate sink, now aragonite, will again reflect BSE (e.g., Gussone et al., 2020). Adding the combined effects from (1)–(3), the upper limit for changing $\delta^{44/40}$Ca values as a result of transient global perturbation is -0.8‰, which would imply that the duration of the excursion was $<10^6$ years, and included the un-

likely combination of increased weathering, ocean acidification, and a change from a calcite to aragonite sea. For comparison, the recovery of the Trezona excursion records a change in $\delta^{44/40}$Ca values of $\sim$ 0.85‰ on all three continents across $\sim$250 m of stratigraphy, while the downturn records a change of $\sim$-1‰ in Namibia across 40–80 m.

The three features discussed above indicate that the $\delta^{44/40}$Ca excursion is unlikely to reflect a global Ca-cycle perturbation. The implication for the carbon isotope record is that the Trezona excursion may predominantly reflect changes in local platform conditions and diagenesis, with aragonite burial in some depositional settings, while other possibly larger carbonate sinks were calcite or dolomite. Alternatively, the processes driving changes in $\delta^{44/40}$Ca and $\delta^{13}$C values would have to be decoupled, for example, with $\delta^{44/40}$Ca values recording changes in diagenesis and mineralogy while $\delta^{13}$C isotopes are recording global seawater chemistry. This latter scenario cannot be ruled out, but carbonate $\delta^{13}$C and $\delta^{44/40}$Ca are modified at broadly similar fluid-to-rock ratios (Ahm et al., 2018), and it is unlikely that carbonate $\delta^{44/40}$Ca values are altered while $\delta^{13}$C values are preserved. Below we use a numerical model of diagenesis to evaluate to what degree these signals may instead be influenced by changes in mineralogy, diagenesis (fluid- versus sediment buffered diagenesis), and the local depositional environment.

### *4.2. Effects of mineralogy, diagenesis, and dolomitization*

In modern platform settings, carbonate $\delta^{13}$C and $\delta^{44/40}$Ca values do not track global seawater chemistry (Swart, 2008; Higgins et al., 2018). Carbon isotope values span from -10 to +7‰ (Swart , 2015; Geyman and Maloof, 2019), and $\delta^{44/40}$Ca values vary between -1.6 and -0.2‰ (Higgins et al., 2018).

Today we accept that these modern platform carbonates do not represent the average carbonate sink and that the geochemical changes largely reflect local changes in mineralogy and diagenesis. To what degree are Cryogenian platform carbonates affected by similar common local processes?

#### *4.2.1. Cryogenian platform aragonite*

The carbonates hosting the Trezona excursion record covariation between Sr/Ca and $\delta^{44/40}$Ca values that is consistent with alteration of platform aragonite across a continuum of fluid- to sediment-buffered conditions (Fig. 6A). Modern platform settings show a similar correlation that reflects mixing between three different carbonate end-members (Higgins et al., 2018): (1) platform aragonite with high Sr/Ca ratios (∼10-12 mmol/mol) and low $\delta^{44/40}$Ca values (∼-1.5‰), (2) fluid-buffered neomorphosed or dolomitized carbonate with low Sr/Ca ratios and high $\delta^{44/40}$Ca that approach modern seawater (0‰), and (3) sediment-buffered neomorphosed calcite (former aragonite), that has retained low $\delta^{44/40}$Ca values (∼-1.5‰) and relatively high Sr/Ca values (∼2-4 mmol/mol).

Calcium isotopes and Sr/Ca ratios are fingerprints of different diagenetic end-members because the Ca isotope fractionation factor and Sr partitioning are sensitive to both mineralogy and precipitation rate (Tang et al., 2008; Gussone et al., 2005). Primary aragonite is more depleted in $^{44}$Ca and enriched in Sr (-1.5‰ and 10 mmol/mol) relative to primary calcite (-1‰ and ∼1 mmol/mol). Diagenetic calcite or dolomite is characterized by lower Sr contents (<1 mmol/mol) and less fractionated $\delta^{44/40}$Ca values, approaching ∼0‰ at equilibrium with the pore-fluids (Fantle and DePaolo, 2007; Jacobson and Holmden, 2008).

In the carbonates that record the Trezona excursion, no primary aragonite is preserved, and instead we interpret the correlation between Sr/Ca ratios and $\delta^{44/40}$Ca as reflecting mixing between fluid- and sediment-buffered end-members. The combination of high Sr/Ca ratios and low $\delta^{44/40}$Ca values excludes the possibility of diagenetic alteration from either marine (would increase $\delta^{44/40}$Ca towards seawater values, Higgins et al., 2018) or meteoric fluids (would lower Sr/C ratios, Allan and Matthews, 1982), and instead indicates sediment-buffered diagenesis of former aragonite (Fig. 6A). The interpretation of precursor aragonite also is supported by petrographic observations of aragonitic ooid fabrics in the Trezona Formation in South Australia (Singh, 1987).

Across the excursion, two separate stratigraphic intervals record sediment-buffered neomorphism of former aragonite. First, pre-excursion carbonate with high $\delta^{13}$C of up to +10‰ (Keele peak), and second, in the nadir of the excursion (Fig. 6C). It is likely that these extreme $\delta^{13}$C values of the Keele peak and Trezona nadir record the chemistry of the environment where the aragonite sediments originally precipitated. In contrast, the intermediate strata that record the downturn and recovery of the Trezona excursion likely were altered during early fluid-buffered diagenesis, and record the chemistry of the early diagenetic pore-waters (Fig. 6C).

In addition to evidence for early diagenesis, there is geochemical evidence for late-stage alteration. While $\delta^{44/40}$Ca and $\delta^{13}$C values are altered at broadly similar fluid-to-rock ratios, $\delta^{18}$O values remain sensitive to diagenesis in settings where both calcium and carbon are sediment-buffered (Banner and Hanson, 1990; Ahm et al., 2018). In other words, it is possible

to have carbonate that has retained primary $\delta^{44/40}$Ca and $\delta^{13}$C values, while $\delta^{18}$O values have been reset during late-stage diagenesis (Ahm et al., 2018). For example, aragonite that was deposited in the Trezona nadir was not significantly altered during early marine or meteoric diagenesis, and therefore preserved low $\delta^{44/40}$Ca values and high Sr/Ca ratios. This aragonite, however, eventually recrystallized to low-Mg calcite during burial. At this stage, the pore-fluids were sediment-buffered with respect to calcium, but $\delta^{18}$O values were reset to lower and more variable values (down to -15‰, Fig. 6D) due to the increase in burial temperature (∼100°C, if assuming fluid values of 0‰ V-SMOW, Kim and O'Neil, 1997). In contrast, carbonate that was dolomitized and stabilized during early marine diagenesis was more resistant to late-stage alteration and $\delta^{18}$O values are less altered (values up to -1‰, Fig. 6D). Although it is possible to alter $\delta^{13}$C values during late-stage burial (Derry, 2010), the correlation between very depleted $\delta^{44/40}$Ca and $\delta^{13}$C values indicates that the deep burial pore-fluids were highly buffered by carbonate dissolution, and sediment-buffered with respect to both calcium and carbon.

*4.2.2. Dolomitization and fluid-buffered diagenesis*

Intervals of early fluid-buffered diagenesis are observed during the downturn and recovery of the Trezona excursion, and in Namibia these intervals are associated with dolomitization. In addition to high $\delta^{44/40}$Ca values and low Sr/Ca ratios, the fluid-buffered dolostone is characterized by relatively low $\delta^{26}$Mg values. Dolostone that formed during early diagenesis under fluid-buffered conditions tend to have lower and less variable $\delta^{26}$Mg values than dolostone forming in sediment-buffered conditions (Fantle and Higgins, 2014; Blättler et al., 2015). These trends are the product of a ∼-2‰ isotopic

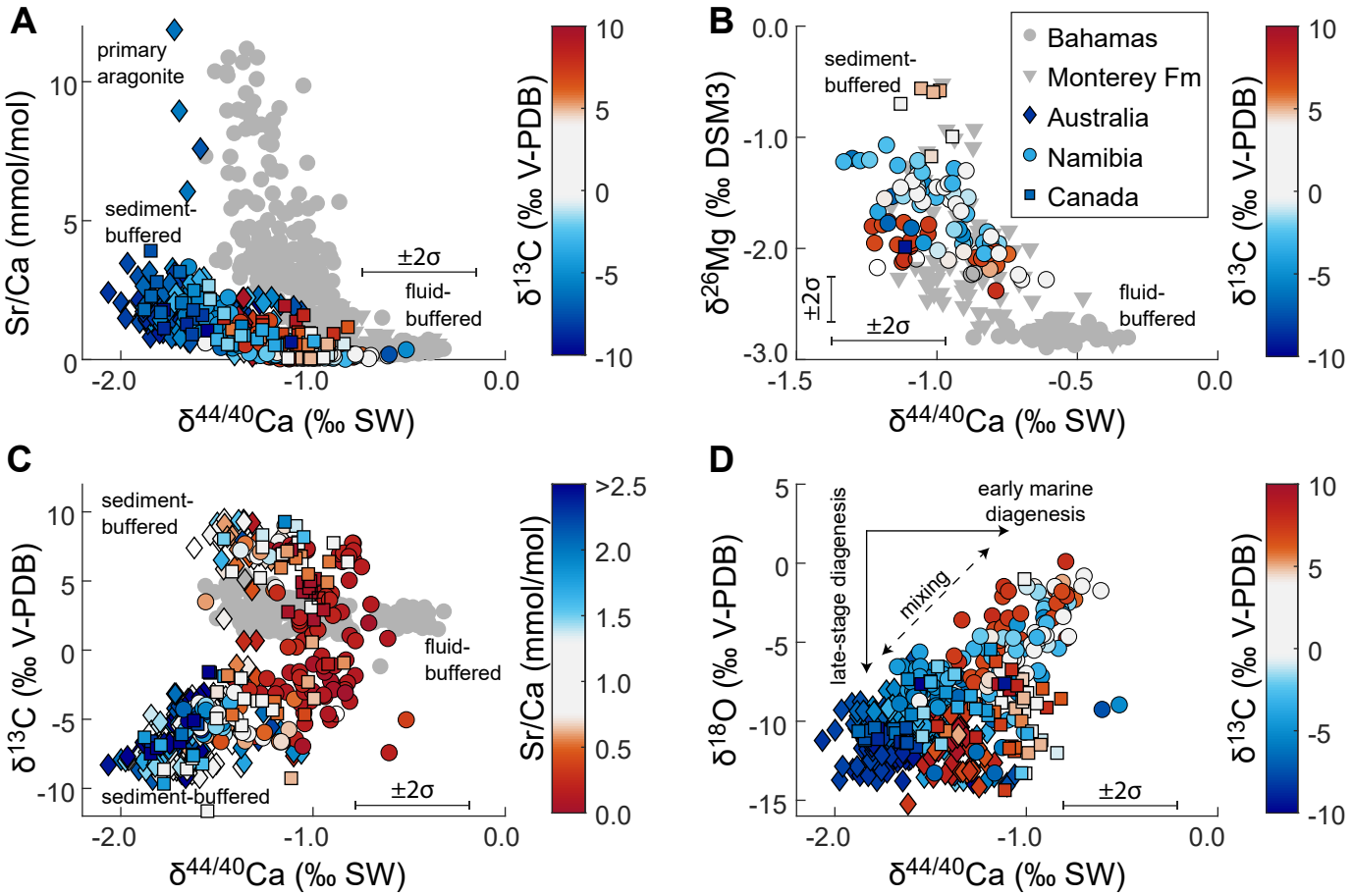


Figure 6: Cross-plots of geochemical data from South Australia, Namibia, and Northwest Canada, in comparison tp platform and periplatform carbonates from the Bahamas and authigenic dolostone from the Neogene Monterey Formation (gray symbols, Blättler et al., 2015; Higgins et al., 2018; Ahm et al., 2018). **A** The correlation between high Sr/Ca ratios and low $\delta^{44/40}$Ca values suggest that the Trezona-bearing strata originated as aragonite that were neomorphosed during sediment-buffered conditions, preserving much of the original geochemistry, including $\delta^{13}$C values. In contrast, high $\delta^{44/40}$Ca values and low Sr/Ca ratios indicate neomorphism or dolomitization under fluid-buffered conditions where the carbonate geochemistry was reset toward the value of the diagenetic fluid. **B** The correlation between high $\delta^{26}$Mg and low $\delta^{44/40}$Ca values indicate sediment-buffered dolomitization whereas low $\delta^{26}$Mg and high $\delta^{44/40}$Ca values indicate fluid-buffered dolomitization. **C** The correlation between $\delta^{13}$C values and $\delta^{44/40}$Ca shows a link between fluid-buffered diagenesis and less extreme $\delta^{13}$C values versus sediment-buffered diagenesis of platform aragonite and extreme $\delta^{13}$C values. **D** The correlation between $\delta^{18}$O and $\delta^{44/40}$Ca values is consistent with a mixing trend between two end-members: (1) samples that have recrystallized during early diagenesis where both $\delta^{18}$O and $\delta^{44/40}$Ca values are reset towards seawater, and (2) samples that have recrystallized during late-stage diagenesis at higher burial temperatures where $\delta^{44/40}$Ca values are preserved (sediment-buffered) and $\delta^{18}$O values are reset.

fractionation associated with the incorporation of Mg into dolomite (Higgins and Schrag, 2010). For example, fluid-buffered dolostone from the Bahamas platform and Neogene Monterey Formation are offset from modern seawater by -2‰ (values of -2.8‰, Blättler et al., 2015; Higgins et al., 2018). In contrast, sediment-buffered dolostone is enriched in $^{26}$Mg due to Rayleigh-type distillation of the pore-fluid in more closed system settings (Blättler et al., 2015).

Across the Trezona excursion in Namibia, two separate stratigraphic intervals record evidence of fluid-buffered diagenesis (Fig. 8). First, dolostone recording the downturn of the Trezona excursion have high $\delta^{44/40}$Ca values and low $\delta^{26}$Mg values (Fig. 6B). Second, high $\delta^{44/40}$Ca values and low $\delta^{26}$Mg values are recorded in dolostone during the recovery of the Trezona excursion prior to deposition of Marinoan glacial deposits. The relationship between $\delta^{26}$Mg and $\delta^{44/40}$Ca across these two intervals are similar to Bahamian dolostone, but offset towards lower $\delta^{44/40}$Ca values (between -1.4 and -0.6‰) and higher $\delta^{26}$Mg values (between -2.5 and -0.5‰), suggesting that the dolomitizing fluid was enriched in $^{26}$Mg and depleted in $^{44}$Ca relative to modern seawater (Fig. 6B). Furthermore, these fluid-buffered intervals record less extreme $\delta^{13}$C values (between approximately -5 and +5‰, Fig. 6C) in comparison to the intervals characterized by sediment-buffered diagenesis (-10 and +10‰).

Table 1: Comparison of diagenetic model results. Model fits are given as best fit with minimum and maximum uncertainty bounds

| | Downturn fluid | Uncertainty ($\sigma$) | Recovery fluid | Uncertainty ($\sigma$) | Modern Seawater |
|---|---|---|---|---|---|
| $\delta^{26}$Mg (‰) | -0.35 | [-0.4, -0.1] | 0.10 | [-0.05, 0.25] | -0.82 |
| $\delta^{44/40}$Ca (‰) | -0.65 | [-0.68, -0.55] | -0.50 | [-0.65, -0.40] | 0.00 |
| $\delta^{13}$C (‰) | -4.0 | [-6.5, -2.7] | 7.0 | [4.0, 12.5] | 0.0–1.5 |
| DIC/$Ca^{2+}$(mol/mol) | 0.05 | [0.04, 0.19] | 0.4 | [0.2, 0.8] | 0.2 |
| $Mg^{2+}$/$Ca^{2+}$(mol/mol) | 0.6 | [0.4, 1.1] | 1.1 | [1.0, 2.0] | 5.1 |

We use a numerical model of early diagenesis to estimate the composition and origin of the diagenetic fluids that dolomitized the Ombaatjie Formation, recording the downturn of the Trezona excursion (Fig. 7). Model results indicate that primary platform aragonite with high $\delta^{13}$C values (estimated at +10‰) were dolomitized by a fluid with $\delta^{13}$C values of -4‰ (uncertainty from -6.5 to -2.7‰). In addition, the model estimates fluid $\delta^{44/40}$Ca values of -0.65‰ and $\delta^{26}$Mg values of -0.35‰ (uncertainty of -0.68 to -0.55‰ and -0.4 to -0.1‰, respectively, Table 1).

Platform fluids can be modified from their original seawater compositions due to reactions in the subsurface and subsequent mixing with freshwater. For example, the low $\delta^{44/40}$Ca values of the downturn fluid (Fig. 7F) are consistent with modern observations from restricted platform settings influenced by submarine groundwater discharge and subsurface carbonate dissolution (∼-1.0 to -0.4‰, Holmden et al., 2012a; Shao et al., 2018). Similarly, subsurface reactions can modify fluid $\delta^{26}$Mg values and $Mg^{2+}/Ca^{2+}$ ratios. Generally, submarine groundwater discharge and carbonate dissolution lead to lower Mg isotope values (Jacobson et al., 2010; Shirokova et al., 2013), while high $\delta^{26}$Mg values are associated with lagoonal and hypersaline environments that are dominated by evaporation and dolomitization (Shirokova et al., 2013). The model results indicate that the diagenetic fluid responsible for dolomitization in the Ombaatjie Formation had both low $Mg^{2+}/Ca^{2+}$ ratios and relative low $\delta^{26}$Mg values (Table 1), consistent with platform waters influenced by submarine groundwater discharge enriched in $^{40}$Ca and $^{24}$Mg due to carbonate dissolution (Fig. 7).

The fluid-buffered interval recording the recovery of the Trezona excur-

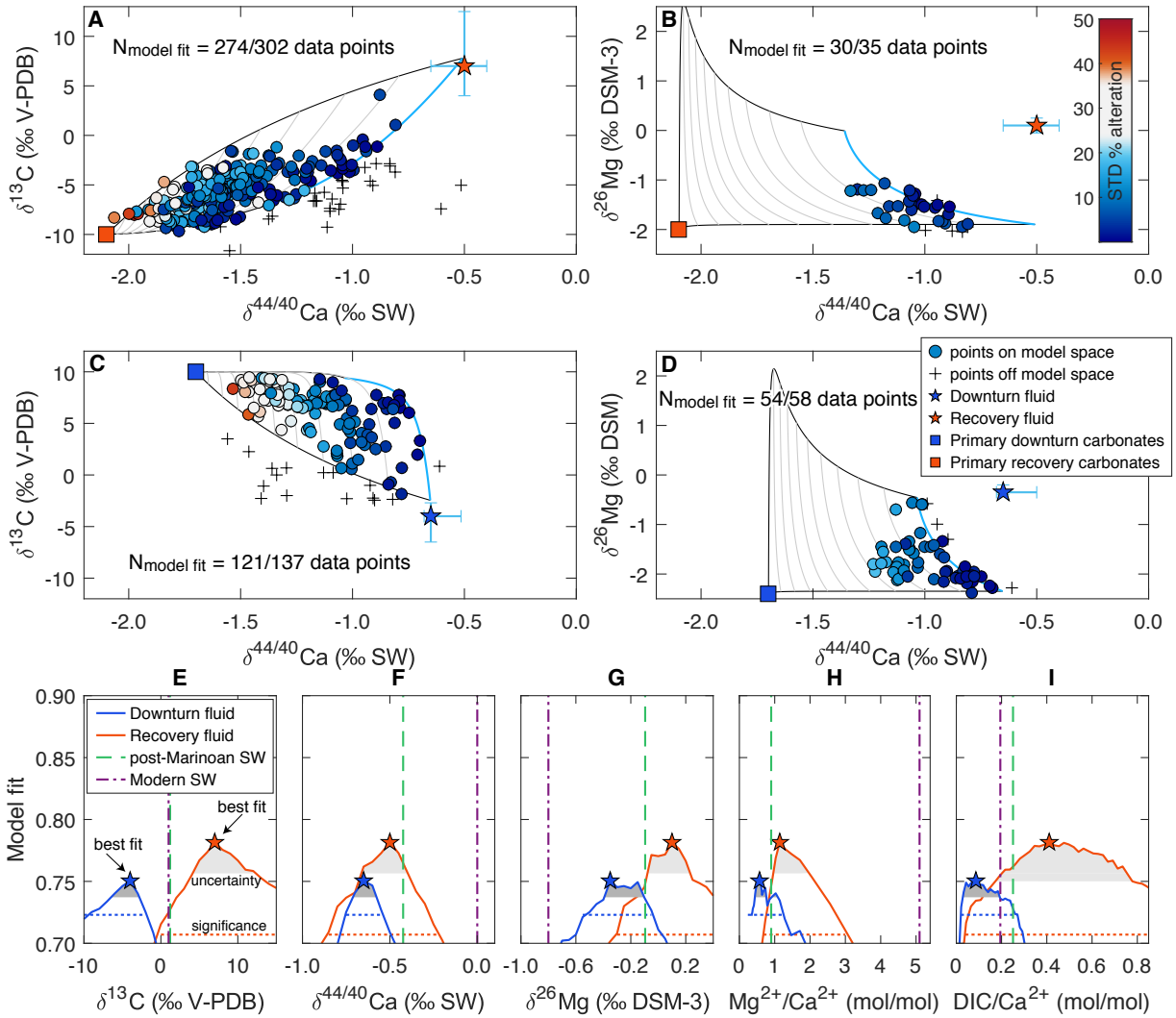


Figure 7: Numerical diagenetic model fits to the Trezona data. Top panels (**A, B**) depict the best model fit to data from the recovering limb of the Trezona excursion (recovery fluid). The middle panels (**C, D**) show the best model fit to data from the downturn of the Trezona excursion (the downturn fluid). Data points are colored by their standard deviation of the modeled percent alteration. In other words, red data points are not well explained by the diagenetic model. The bottom panels (**E–I**), show the results for the model optimization with the best fit value. The grey area shows the uncertainty level of the model cost when accounting for the uncertainty of the data (66th percentile). The significance level represents the 95th percentile of model fits to randomly generated data (see methods for details). For comparison, modern seawater (e.g., Higgins et al., 2018) and re-calculated model results for post-Marinoan seawater also are plotted (basal Ediacaran cap carbonates, Ahm et al., 2019).

sion is observed on three separate continents (Table 1). Across this interval, model results indicate that primary platform aragonite with low $\delta^{13}$C values (estimated at -10‰) was dolomitized and/or neomorphosed by a fluid with $\delta^{13}$C values of +7‰, with an uncertainty range of +4 to +12.5‰. In addition, the model estimates fluid $\delta^{44/40}$Ca values of -0.5‰ and $\delta^{26}$Mg values of +0.1‰ (uncertainty of -0.65 to -0.40‰, and -0.05 to +0.25‰, respectively, Table 1).

The fact that a single diagenetic fluid may explain the trends observed during the recovery of the Trezona excursion on three continents could indicate a possible late Cryogenian seawater origin (Fig. 7). Fluid $\delta^{44/40}$Ca values of -0.5‰ would suggest more $^{44}$Ca-depleted seawater relative to today, which is consistent with estimates of pre mid-Mesozoic seawater, prior to a deep-marine carbonate reservoir (Akhtar et al., 2020). However, the low fluid $\delta^{44/40}$Ca values also are within range of modern observations of restricted platform waters that are offset from modern seawater (Holmden et al., 2012a; Shao et al., 2018). Our results therefore cannot show conclusively that the 'recovery fluid' represents open-ocean seawater, but the relatively high $\delta^{44/40}$Ca values suggests a somewhat modified seawater origin. If the $\delta^{26}$Mg value and $Mg^{2+}/Ca^{2+}$ ratio of the recovery fluid provide a close estimate of Cryogenian seawater (0.1‰ and 1.1 mol/mol, respectively, Fig. 7G), then seawater was significantly enriched in $^{26}$Mg and had lower $Mg^{2+}/Ca^{2+}$ ratios relative to the modern (modern values of -0.8‰ and 5.1 mol/mol, respectively, e.g., Higgins et al., 2018).

### *4.3. The Trezona excursion as a local phenomenon linked to siliciclastic input*

On continent fringing platforms, mixed deposition of carbonate and siliciclastic sediments is influenced by regional climate and local factors such as sediment and nutrient influx from river drainage systems that meander, avulse, and reorganize. Changing inputs of siliciclastic material can drive changes in platform water-depth, affecting platform fluid circulation, due to differences in permeability, porosity, and in the changing size of the freshwater lens. For example, an increase in siliciclastic input often suffocates carbonate production, leading to a decrease in sediment accumulation rate relative to subsidence rate, and increases platform water-depth (Schlager, 1989). An increase in local sea-level can drive upwelling of deep-seated groundwater from the platform interior as thermally-driven circulation increases and pore-fluids are pushed upwards (Kohout et al., 1977). In contrast, reducing the supply of siliciclastic material often allows carbonate accumulation to keep up with subsidence rate, decreasing platform water-depth and expanding the freshwater lens in platform interiors. As the less dense freshwater flows seawards, it drives an increase in the deeper compensating flow of seawater into platforms (Henderson et al., 1999). Reorganization of rivers can change, not only the platform water depth and subsurface fluid flow, but also the chemical composition of the coastal surface waters (inputs of siliciclastics, nutrients, alkalinity, and remineralized organic carbon) and therefore the $\delta^{13}$C of carbonate precipitated from them (Lapointe et al., 1992; Patterson and Walter, 1994).

#### *4.3.1. Cryogenian $^{13}C$ enriched platform aragonite*

On all three continents, the interval preceding the Trezona excursion is characterized by a high fraction of carbonate relative to siliciclastic material, with high carbonate $\delta^{13}$C values (∼+10‰, Fig 8, panel 1). Calcium isotopes and Sr/Ca ratios indicate that these stata originally were primary aragonite. High $\delta^{13}$C values in Cryogenian platform surface waters may reflect generally high Cryogenian seawater $\delta^{13}$C values, but we speculate that at least part of this enrichment is related to a combination of elevated primary productivity and diurnal cycling in microbial mat dominated platform environments (Geyman and Maloof, 2019). The combination of low $\delta^{44/40}$Ca (<-1‰) and high $\delta^{13}$C values imply that these $^{13}$C-enriched intervals cannot represent the average carbonate sink and need to be balanced by the burial of $^{44}$Ca enriched (and possibly more $^{13}$C depleted) carbonate in other localities.

#### *4.3.2. The Trezona excursion*

The downturn of the Trezona excursion only is recorded in dolostone in Namibia, while in other localities pre-Trezona carbonate gives way to siliciclastic strata (Fig. 8, panel 2). In Namibia, we hypothesize that progressive platform drowning is responsible for a temporary increase in platform fluid-flow that resulted in dolomitization of the underlying carbonate (parasequence b7, Fig. 4). This phase of dolomitization declines in intensity in concert with the decline in $\delta^{13}$C values towards the nadir. The model results suggest that the pore-fluids generated from re-circulating platform waters had $\delta^{13}$C values ∼-4‰ (Table 1), likely due to subsurface mixing between platform surface waters (more $^{13}$C-depleted, see below) and upwelling seawater (open-ocean, less $^{13}$C-depleted).

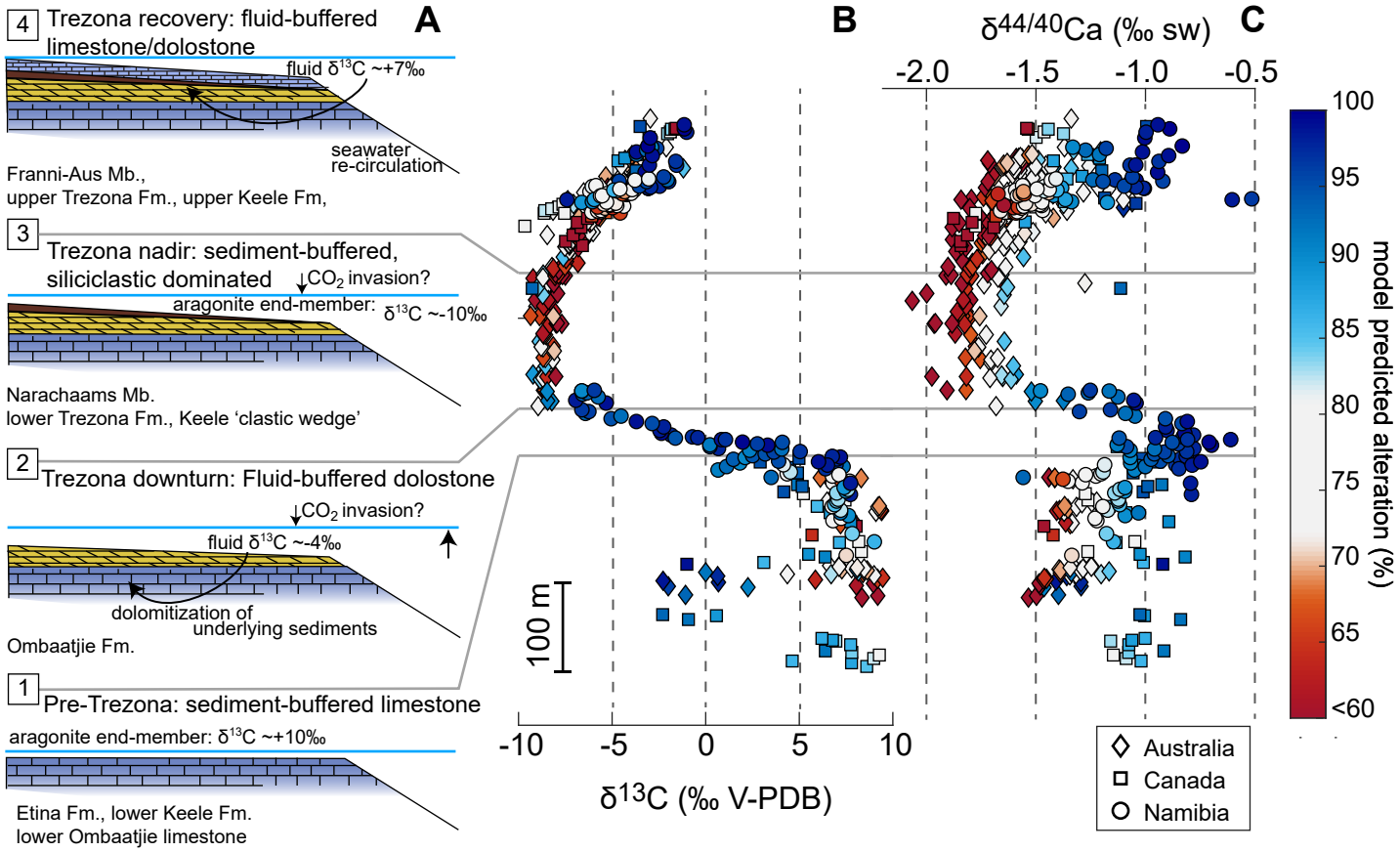


Figure 8: **A.** Interpretation of primary and diagenetic end-members observed across the Trezona excursion. Cryogenian carbonates record changes in the diagenetic regime between fluid- to sediment-buffered that consistently correlate with prominent stratigraphic markers and changes in $\delta^{13}$C values. (1) The interval preceding the Trezona excursion is characterized by shallow-water carbonate with $\delta^{13}$C values $\sim$+10‰ in former aragonitic sediments. (2) The downturn of the Trezona excursion is recorded by a decrease in $\delta^{13}$C values and is only observed in Namibia. The downturn is interpreted as a result of fluid-buffered dolomitization of the underlying sediment associated with drowning of the Ombaatjie platform. (3) The nadir of the excursion is marked by deposition of siliciclastic stata and a reduction in fluid-flow, resulting in the preservation of former platform aragonite with $\delta^{13}$C values $\sim$-10‰. (4) The recovery of the excursion is associated with an increase in carbonate deposition relative to siliciclastic, correlating with increasing $\delta^{13}$C values. This interval also records increased fluid-buffered diagenesis of platform sediments. **B.** $\delta^{13}$C values and **C.** $\delta^{44/40}$Ca values are colored by the predicted degree of alteration from the diagenetic model.

Although the downturn of the Trezona excursion is observed only in Namibia, low $\delta^{13}$C values (between -7 and -10‰) are observed in former aragonite in the nadir of the Trezona excursion worldwide. These observations suggest that $\delta^{13}$C values of DIC in platform water, where aragonite likely precipitated, shifted from high to low in concert with increasing siliciclastic relative to carbonate input. The nadir of the Trezona excursion is recorded in settings where aragonite is interbedded with fine-grained siliciclastic sediments, decreasing permeability and possibly protecting the aragonite from early diagenesis (Fig. 8, panel 3).

The driving mechanism for generating extremely depleted $\delta^{13}$C values in Cryogenian surface waters remains enigmatic, but our analysis indicates a link to siliciclastic input and a strong diurnal engine in platform surface waters (with background $\delta^{13}$C values of >+7‰). We speculate that an increase in the input of siliciclastic sediments from river drainage may be associated with an influx of nutrients, which could lead to a localized burst in productivity of microbial mats (Lapointe et al., 1992). Increased microbial productivity provides a possible link to the extremely depleted $\delta^{13}$C values observed in the Trezona nadir. In modern hypersaline ponds dominated by microbial mats, periods of intense productivity have been associated with low $\delta^{13}$C values of DIC (<-10‰, Lazar and Erez, 1992). These low values are a product of kinetic isotopic fractionation during $CO_2$ hydration (estimated kinetic fractionation factors ∼-11‰, Zeebe and Wolf-Gladrow, 2001). In other words, while surface water DIC concentrations are significantly depleted due to high productivity rates, $CO_2$ is replenished by the relatively slow invasion from the atmosphere, which is associated with a large negative

carbon isotope fractionation (Lazar and Erez, 1992).

There are some important differences between the modern hypersaline ponds (Lazar and Erez, 1992) and the Cryogenian platform environments. First, while the modern ponds are hypersaline, there is no evidence for evaporites in the Cryogenian successions. Second, in the modern ponds, carbonate precipitation is limited during the most extreme periods of disequilibrium, because the invasion of $CO_2$ decreases carbonate saturation (Lazar and Erez, 1992). However, $CO_2$ invasion has been connected to rapid carbonate precipitation in alkaline environments with a high supply of $Ca^{2+}$ (Clark et al., 1992). In these environments, subsurface fluids with very low DIC/$Ca^{2+}$ ratios come into contact with the atmosphere, resulting in rapid invasion of $CO_2$ and precipitation of carbonates with $\delta^{13}C$ values down to -25‰ (Clark et al., 1992). We imagine that Cryogenian platform waters were poised somewhere in-between these modern end-members, consistent with model results of low DIC/$Ca^{2+}$ ratios in the 'downturn fluid' (Table 1). Additionally, while hypersalinity promotes disequilibrium due to very slow rates of air-sea gas exchange, disequilibrium also has been observed in freshwater lakes during intense algal blooms where rates of productivity exceed rates of $CO_2$ invasion (Herczeg and Fairbanks, 1987). We therefore speculate that Cryogenian platform environments dominated by microbial mats and associated with high background diurnal productivity (as evidence by background $\delta^{13}C$ values of up to +10‰), may be poised close to a disequilibrium threshold where the kinetic effects of $CO_2$ invasion could be readily expressed. In this world, the Trezona excursion captures a period where an increase in siliciclastic influx drove platform surface water across this threshold, resulting in $\delta^{13}C$ values

of ∼-10‰.

*4.3.3. The Trezona recovery*

Following the nadir of the Trezona excursion, platform carbonate $\delta^{13}$C eventually recovers before the onset of the Marinoan glaciation. On all three continents, this interval is characterized by an increase in carbonate deposition relative to siliciclastics, and coincides with increasing fluid-buffered diagenesis (Fig. 8, panel 4). As carbonate input increased and accommodation space diminished, platform water-depth decreased, the fresh-water lens expanded, and seawater re-circulation in platforms intensified (Fig. 8, panel 4). An increase in fluid-flow across this coarsening upwards succession is consistent with observations of fluid-flow patterns from the Bahamas where periods of relative sea-level fall are characterized by increased aragonite neomorphism and dolomitization (Vahrenkamp et al., 1991; Melim et al., 2002).

The late-Cryogenian 'recovery fluid' responsible for widespread diagenetic resetting of platform carbonate had a $\delta^{13}$C value of ∼+7‰, and most likely reflects the composition of platform surface waters that have returned to pre-Trezona conditions (from being $^{13}$C-depleted to $^{13}$C-enriched, Fig. 8, panel 4).

*4.4. Local platform signals and global mass balance*

The prevalence of local geochemical signals in Cryogenian carbonate successions have implications for the global mass balance of both carbon and calcium, and the degree to which the platform carbonates represent the average carbonate sink. An important observation is that the majority of carbonates measured in this study have $\delta^{44/40}$Ca values that are lower than BSE (-1‰,

Skulan et al., 1997), and mass balance requires that these low $\delta^{44/40}$Ca values are balanced by the precipitation of $^{44}$Ca enriched carbonates elsewhere (Blättler and Higgins, 2017). As the geological records is incomplete, it is not possible to show conclusively where this sink should be. One possibility is authigenic carbonate and cements, which tend to have high $\delta^{44/40}$Ca values (Blättler et al., 2015; Schrag et al., 2013). Another possibility is the precipitation of carbonate veins during hydrothermal alteration of basalt (Bjerrum and Canfield, 2004). A third possibility is to reexamine the extent to which the Trezona excursion is observed in Cryogenian strata globally. For example, the excursion is not observed in the Cryogenian carbonate-dominated successions of Mongolia and Panamints Range, Death Valley (Bold et al., 2020; Prave et al., 1999), which previously has been interpreted as a result of sub-glacial erosion (Bold et al., 2016). Alternatively, it is possible that these platforms simply did not reach a disequilibrium threshold where $\delta^{13}$C values switch to -10‰, and due to relatively less siliciclastic input, also remained more susceptible to early diagenesis and fluid-buffered alteration. Mass balance could be achieved if fluid-buffered intervals characterized by high $\delta^{44/40}$Ca values (and less extreme $\delta^{13}$C values closer to ∼0‰) were correlated with sediment-buffered intervals characterized by low $\delta^{44/40}$Ca (and more extreme $\delta^{13}$C values, ∼+10 and -10‰). These intervals would not have been correlated previously due to the practice of using carbon isotope stratigraphy in Cryogenian successions.

Another feature of our hypothesis is that it suggests that the correlation between siliciclastic input and negative $\delta^{13}$C excursions in platform aragonite could be a common Neoproterozoic phenomenon during periods of high

background diurnal carbon cycling (baseline $\delta^{13}$C>+5‰). Indeed, other excursions such as the Shuram-Wonoka, the Taishir, and the Islay anomaly are associated with a change from $^{13}$C-enriched to $^{13}$C-depleted carbonate, coinciding with a fractional increase in siliciclastic material (e.g., Husson et al., 2015; Bold et al., 2016; Park et al., 2019). It may be possible to change global siliciclastic fluxes though either global climate change or rapid glacio-eustatic sea-level rise, although currently there is no evidence for land-based ice-sheets in the Cryogenian 'non-glacial interlude'. Alternatively, in modern mixed platform environments, the influx of siliciclastic material largely is controlled by stochastic fluvial-deltaic and tectonic processes that operate on timescales from thousands to millions of years. If similar local processes are operating in Cryogenian mixed carbonate-siliciclastic platforms and contributing to the switch to negative $\delta^{13}$C values, it would be consistent with the lack of the Trezona excursion in some Cryogenian successions (e.g., Mongolia and Panamint Range) and the lack of the Taishir anomaly in others (e.g., Australia, Namibia, Northwest Canada). Moreover, in the localities where the excursion is found, it is not yet clear if it correlates across continents on time-scales that are relevant for the global carbon and calcium cycle ($<10^5 - 10^6$ years). Strontium isotope ratios and glacial diamictite-cap carbonate lithostratigraphical correlations broadly constrain the Trezona excursions within ∼10 Myr (Fig. 1), but these correlation tools do not provide the resolution to confirm that these excursions are coeval. Instead, it is possible that the switch from $^{13}$C-enriched to $^{13}$C-depleted carbonate on local platforms occurred separately across a broader period (e.g., between 1–5 Myrs), where global climate and tectonics contributed to a, locally variable,

increased flux of siliciclastic material to platform environments.

## 5. Conclusions

This study demonstrates that stratigraphic changes in Cryogenian platform carbonate $\delta^{13}$C values are characterized by intervals of fluid-versus sediment-buffered diagenesis linked to changes in the relative input of carbonate and siliciclastic sediments. First, the interval preceding the Trezona excursion is characterized by shallow-water conditions with $\delta^{13}$C values of $\sim$+10‰ in former aragonite sediments. Second, in Namibia the downturn of the Trezona excursion correlates with an increase in platform fluid-flow rates, dolomitization of the underlying sediments, and subsequent platform drowning by siliciclastic material. Diagenetic fluids partially are sourced from platform surface waters with exceptionally low $\delta^{13}$C and low $\delta^{44/40}$Ca values. In the nadir of the excursion, fluid-flow is reduced due to the decrease in permeability from interbedded siliciclastics, resulting in sediment-buffered preservation of former platform aragonite with $\delta^{13}$C values of $\sim$-10‰. Finally, the recovery of the Trezona excursion correlates with an increase in carbonate inputs, an increase in platform fluid-flow, and increasing $\delta^{13}$C values of platform sediments. This relationship suggests a mechanistic link between intervals of siliciclastic input and $\delta^{13}$C excursions in Cryogenian platform environments.

## 6. Acknowledgments

This study greatly benefited from reviews by Ashleigh Hood and two anonymous reviewers in addition to discussions with James Busch, Laurence Coogan, Blake Dyer, Emily Geyman, and Jon Husson. We would like to thank Eben Blake Hodgin and Alan Rooney for providing Sr isotope data for sections

from Northwest Canada. We also thank Elizabeth Lundstrom and Nicolas Slater for assistance in the lab at Princeton University. ASCA acknowledges support from The Simons Foundation (SCOL 611878) and The Carlsberg Foundation. ASCA and CJB acknowledge support from the Danish National Research Foundation (Grant No. DNRF53). ACM and CVR acknowledge support from NSF (EAR-0842946) for funding fieldwork on the Trezona Formation in South Australia. JAH acknowledges support from NSF (IES-1410317) and from NSF OCE CAREER Grant (1654571).

## References

Ahm, A-S.C., Bjerrum, C.J., Blättler, C.L., Swart, P.K., Higgins, J.A., 2018. Quantifying early marine diagenesis in shallow-water carbonate sediments. Geochimica et Cosmochimica Acta 236, 140–159. https://doi.org/10.1016/j.gca.2018.02.042

Ahm, A.-S.C., Maloof, A.C., Macdonald, F.A., Hoffman, P.F., Bjerrum, C.J., Bold, U., Rose, C.V., Strauss, J.V., Higgins, J.A., 2019. An early diagenetic deglacial origin for basal Ediacaran "cap dolostones". Earth and Planetary Science Letters 506, 292–307. https://doi.org/10.1016/j.epsl.2018.10.046

Aitken, J.D., 1991. Two late Proterozoic glaciations, Mackenzie Mountains, Northwestern Canada. Geology 19 (5), 445–448. https://doi.org/10.1130/0091-7613(1991)019<0445:TLPGMM>2.3.CO;2

Akhtar, A.A., Santi, L.M., Griffiths, M.L., Becker, M., Eagle, R.A., Kim, S., Kocsis, L., Rosenthal, Y., Higgins, J.A., 2020. A record of the $\delta^{44/40}$Ca

and [Sr] if seawater over the last 100 million years from fossil elasmobranch tooth enamel. Earth and Planetary Science Letters 543, 116354. https://doi.org/10.1016/j.epsl.2020.116354

Allan, J.R., Matthews, R.K., 1982. Isotope signatures associated with early meteoric diagenesis. Sedimentology 29 (6), 797–817. https://doi.org/10.1111/j.1365-3091.1982.tb00085.x

Baldwin, G.J., Turner, E.C., Kamber, B.S., 2016. Tectonic controls on distribution and stratigraphy of the Cryogenian Rapitan iron formation, Northwestern Canada. Precambrian Research 278, 303–322. https://doi.org/10.1016/j.precamres.2016.03.014

Banner, J.L., Hanson, G.N., 1990. Calculation of simultaneous isotopic and trace element variations during water-rock interaction with applications to carbonate diagenesis. Geochimica et Cosmochimica Acta 54 (11), 3123–3137. https://doi.org/10.1016/0016-7037(90)90128-8

Bjerrum, C.J., Canfield, D.E., 2004. New insights into the burial history of organic carbon on the early Earth. Geochemistry, Geophysics, Geosystems 5 (8) https://doi.org/10.1029/2004GC000713

Blättler, C.L., Miller, N.R., Higgins, J.A., 2015. Mg and Ca isotope signatures of authigenic dolomite in siliceous deep-sea sediments. Earth and Planetary Science Letters 419, 32–42. https://doi.org/10.1016/j.epsl.2015.03.006

Blättler, C.L., Higgins, J.A., 2017. Testing Urey's carbonate-silicate cycle using the calcium isotopic composition of sedimentary carbonates. Earth

and Planetary Science Letters 479, 241–251. https://doi.org/10.1016/j.epsl.2017.09.033

Bold, U., Smith, E., Rooney, Al., Bowring, S.A., Buchwaldt, R., Dudás, F., Ramezani, J., Crowley, J.L., Schrag, D. P., Macdonald, F.A., 2016. Neoproterozoic stratigraphy of the Zavkhan terrane of Mongolia: The backbone for Cryogenian and early Ediacaran chemostratigraphic records. American Journal of Science 316, 1–63. https://doi.org/10.2475/01.2016.01

Bold, U., Ahm, A-S.C., Schrag, D.P., Higgins, J.A., Macdonald, F.A., 2020. Effect of dolomitization on isotopic records from Neoproterozoic carbonates in southwestern Mongolia. Precambrian Research 350, 105902. https://doi.org/10.1016/j.precamres.2020.105902

Calver, C., Crowley, J., Wingate, M., Evans, D., Raub, T., Schmitz, M., 2013. Globally synchronous Marinoan deglaciation indicated by U-Pb geochronology of the Cottons Breccia, Tasmania, Australia. Geology 41 (10), 1127–1130. https://doi.org/https://doi.org/10.1130/G34568.1

Clark, I.D., Fontes, J.C., Fritz, P., 1992. Stable isotope disequilibria in travertine from high pH waters: Laboratory investigations and field observations from Oman. Geochimica et Cosmochimica Acta 56 (5), 2041–2050. https://doi.org/https://doi.org/10.1016/0016-7037(92)90328-G

Cox, G.M., Isakson, V., Hoffman, P.F., Gernon, T.M., Schmitz, M.D., Shahin, S., Collins, A.S., Preiss, W., Blades, M.L., Mitchell, R.N.,

Nordsvan, A., 2018. South Australian U-Pb zircon (CA-ID-TIMS) age supports globally synchronous Sturtian deglaciation. Precambrian Research 315, 257–263. https://doi.org/https://doi.org/10.1016/j.precamres.2018.07.007

Crockford, P.W., Kunzmann, M., Blättler, C.L., Boriana, K-A., Murphy, J.G., Ahm, A-S., Sharoni, S., Halverson, G.P., Planavsky, N.J., Halevy, I., Higgins, J.A., 2020. Reconstructing Neoproterozoic seawater chemistry from early diagenetic dolomite. Geology 49 https://doi.org/10.1130/G48213.1

Day, E.S., James, N.P., Narbonne, G.M., Dalrymple, R.W., 2004. A sedimentary prelude to Marinoan glaciation, Cryogenian (middle Neoproterozoic) Keele Formation, Mackenzie Mountains, Northwestern Canada. Precambrian Research 133 (3–4), 223–247. http://dx.doi.org/10.1016/j.precamres.2004.05.004

Derry, L.A., 2010. A burial diagenesis origin for the Ediacaran Shuram-Wonoka carbon isotope anomaly. Earth and Planetary Science Letters 294 (1–2), 152–162. https://doi.org/10.1016/j.epsl.2010.03.022

Fanning, C.M., Link, P.K., 2008. Age constraints for the Sturtian glaciation; data from the Adelaide geosyncline, South Australia and Pocatello Formation, Idaho, USA. Geol. Soc. Aus. Abstracts. Selwyn Symposium, pp. 57–62. https://doi.org/http://dx.doi.org/10.1016/j.gca.2014.07.025

Fantle, M.S., DePaolo, D.J., 2007. Ca isotopes in carbonate sediment and

pore fluid from ODP Site 807A: The $Ca^{2+}$(aq)–calcite equilibrium fractionation factor and calcite recrystallization rates in Pleistocene sediments. Geochimica et Cosmochimica Acta 71 (10), 2524–2546. https://doi.org/http://dx.doi.org/10.1016/j.gca.2007.03.006

Fantle, M.S., Higgins, J.A, 2014. The effects of diagenesis and dolomitization on Ca and Mg isotopes in marine platform carbonates: Implications for the geochemical cycles of Ca and Mg. Geochimica et Cosmochimica Acta 142, 458–481. https://doi.org/http://dx.doi.org/10.1016/j.gca.2014.07.025

Geyman, E.C., Maloof, A.C., 2019. A diurnal carbon engine explains 13C-enriched carbonates without increasing the global production of oxygen. Proceedings of the National Academy of Sciences 116 (49), 24433–24439. https://doi.org/10.1073/pnas.1908783116

Gussone, N., Böhm, F., Eisenhauer, A., Dietzel, M., Heuser, A., Teichert, B. M.A., Reitner, J., Wörheide, G., Dullo, W.C., 2005. Calcium isotope fractionation in calcite and aragonite. Geochimica et Cosmochimica Acta 69 (18), 4485–4494. https://doi.org/http://dx.doi.org/10.1016/j.gca.2005.06.003

Gussone, N., Ahm, A-S.C. Lau, K.V., Bradbury, H.J., 2020. Calcium isotopes in deep time: Potential and limitations. Chemical Geology (544), 119601. https://doi.org/10.1016/j.chemgeo.2020.119601

Halverson, G.P., Hoffman, P.F., Schrag, D.P., Maloof, A.C., Rice, A.H.N., 2005. Toward a Neoproterozoic composite carbon-isotope record. Geologi-

cal Society of America Bulletin 117 (9-10), 1181–1207. https://doi.org/10.1130/b25630.1

Halverson, G.P., Dudas, F.O., Maloof, A.C., Bowring, S.A., 2007. Evolution of the $^{87}Sr/^{86}Sr$ composition of Neoproterozoic seawater. Palaeography, Palaeoclimatology, Palaeoecology 256 (3), 103–129. https://doi.org/10.1016/j.palaeo.2007.02.028

Henderson, G.M., Slowey, N.C., Haddad, G.A., 1999. Fluid flow through carbonate platforms: constraints from $^{234}U/^{238}U$ and $Cl^-$ in Bahamas porewaters. Earth and Planetary Science Letters 169 (1–2), 99–111. https://doi.org/http://dx.doi.org/10.1016/S0012-821X(99)00065-5

Herczeg, A.L., Fairbanks, R.G., 1987. Anomalous carbon isotope fractionation between atmospheric $CO_2$ and dissolve inorganic carbon induces by intense photosynthesis. Geochimica et Cosmochimica Acta 51 (4), 895–899. https://doi.org/10.1016/0016-7037(87)90102-5

Higgins, J.A., Schrag, D.P., 2010. Constraining magnesium cycling in marine sediments using magnesium isotopes. Geochimica et Cosmochimica Acta 74 (17),5039–5053. https://doi.org/http://dx.doi.org/10.1016/j.gca.2010.05.019

Higgins, J.A., Blättler, C.L., Lundstrom, E.A., Santiago-Ramos, D., Akhtar, A., Ahm, A.S.C., Bialik, O., Holmden, C., Bradbury, H., Murray, S.T., Swart, P., 2018. Mineralogy, early marine diagenesis, and the chemistry of shallow water carbonate sediments. Geochimica et Cosmochimica Acta 220, 512–534. https://doi.org/10.1016/j.gca.2017.09.046

Hoffman, P.F., Kaufman, A.J., Halverson, G.P., Schrag, D.P., 1998. A Neoproterozoic Snowball Earth. Science 281 (5381), 1342–1346. https://doi.org/10.1126/science.281.5381.1342

Hoffman, P.F., Schrag, D.P., 2002. The Snowball Earth hypothesis: testing the limits of global change. Terra Nova 14 (3), 129–155. https://doi.org/10.1046/j.1365-3121.2002.00408.x

Hoffman, P.F., 2011. Strange bedfellows: glacial diamictite and cap carbonate from the Marinoan (635 Ma) glaciation in Namibia. Sedimentology 58 (1), 57–119. https://doi.org/10.1111/j.1365-3091.2010.01206.x

Hoffmann, K.-H., Condon, D., Bowring, S., Crowley, J., 2004. U-Pb zircon date from the Neoproterozoic Ghaub Gormation, Namibia: Constraints on Marinoan glaciation. Geology 32 (9), 817–820. https://doi.org/10.1130/g20519.1

Holmden, C., Papanastassiou, D.A., Blanchon, P., Evans, S., 2012. $\delta^{44/40}$Ca variability in shallow water carbonates and the impact of submarine groundwater discharge on Ca-cycling in marine environments. Geochimica et Cosmochimica Acta 83, 179–194. https://doi.org/https://doi.org/10.1016/j.gca.2011.12.031

Holmden, C., Panchuk, K., Finney, S.C., 2012. Tightly coupled records of Ca and C isotope changes during the Hirnantian glaciation event in an epeiric sea setting. Geochimica et Cosmochimica Acta 98, 94–106. https://doi.org/10.1016/j.gca.2012.09.017

Husson, J.M., Higgins, J.A., Maloof, A.C., Schoene, B., 2015. Ca and Mg isotope constraints on the origin of Earth's deepest C excursion. Geochimica et Cosmochimica Acta 160, 243–266. https://doi.org/http://dx.doi.org/10.1016/j.gca.2015.03.012

Jacobson, A.D., Holmden, C., 2008. $\delta^{44}$Ca evolution in a carbonate aquifer and its bearing on the equilibrium isotope fractionation factor for calcite. Earth and Planetary Science Letters 270 (3–4), 349–353. https://doi.org/http://dx.doi.org/10.1016/j.epsl.2008.03.039

Jacobson, A.D., Zhang, Z., Lundstrom, C., Huang, F., 2010. Behavior of Mg isotopes during dedolomitization in the madison aquifer, South Dakota. Earth and Planetary Science Letters 297 (3), 446–452. https://doi.org/https://doi.org/10.1016/j.epsl.2010.06.038

Kaufman, A.J., Knoll, A.J., Narbonne G.M., 1997. Isotopes, ice ages, and terminal Proterozoic earth history. PNAS 94, 6600–6605. https://doi.org/10.1073/pnas.94.13.6600

Kendall, B., Creaser, R.A., Selby, D., 2006. Re-Os geochronology of post-glacial black shales in australia: Constraints on the timing of "sturtian" glaciation. Geology 34 (9), 729–732. https://doi.org/10.1130/g22775.1

Kim, S-T., O'Neil, J.R., 1997. Equilibrium and nonequilibrium oxygen isotope effects in synthetic carbonates. Geochimica et Cosmochimica Acta 61 (16), 3461–3475. https://doi.org/10.1016/S0016-7037(97)00169-5

Klaebe, R., Kennedy, M., 2019. The palaeoenvironmental context of the Trezona anomaly in South Australia: Do carbon isotope values record a global or regional signal? The Depositional Record 5(1), 131–146.

Kohout, F.A., Henry, H.R., Banks, J.E., 1977. Hydrogeology related to geothermal conditions of the Floridan Plateau FL Bur. Geol. Spec. Publ., 21, 1–39.

Komar, N., Zeebe, R.E., 2016. Calcium and calcium isotope changes during carbon cycle perturbations at the end-Permian. Paleoceanography 31 (1), 115–130. https://doi.org/10.1002/2015PA002834

Lapointe, B.E., Litter, M.M., Litter, D.S., 1992. Nutrient availability to marine macroalgae in siliciclastic versus carbonate-rich coastal waters. Esturies 15 (1), 75–82. https://doi.org/10.2307/1352712

Lazar, B., Erez, J., 1992. Carbon geochemistry of marine-derived brines: I. $^{13}$C depletions due to intense photosynthesis. Geochimica et Cosmochimica Acta 56(1), 335–345. https://doi.org/http://dx.doi.org/10.1016/0016-7037(92)90137-8

Macdonald, F.A., Schmitz, M.D., Crowley, J.L., Roots, C.F., Jones, D.S., Maloof, A.C., Strauss, J.V., Cohen, P.A., Johnston, D.T., Schrag, D.P., 2010. Calibrating the Cryogenian. Science 327(5970), 1241–1243. https://doi.org/10.1126/science.1183325

Macdonald, F.A., Schmitz, M.D., Strauss, J.V., Halverson, G.P., Gibson, T.M., Eyster, A., Cox, G., Mamrol, P., Crowley, J.L., 2018. Cryogenian

of Yukon. Precambrian Research 319, 114–143. https://doi.org/https://doi.org/10.1016/j.precamres.2017.08.015

McKirdy, D.M., Burgess, J.M., Lemon, N.M., Yu, X., Cooper, A.M., Gostin, V.A., Jenkins, R. J.F., Both, R.A., 2001. A chemostratigraphic overview of the late Cryogenian interglacial sequence in the Adelaide fold-thrust belt, South Australia. Precambrian Research 106 (1–2), 149–186. https://doi.org/http://dx.doi.org/10.1016/S0301-9268(00)00130-3

Melim, L.A., Westphal, H., Swart, P.K., Eberli, G.P., Munnecke, A., 2002. Questioning carbonate diagenetic paradigms: evidence from the Neogene of the Bahamas. Marine Geology 185 (1–2), 27–53. https://doi.org/http://dx.doi.org/10.1016/S0025-3227(01)00289-4

Park, Y., Swanson-Hysell, N.L., MacLennan, S.A., Maloof, A.C., Gebreslassie, M., Tremblay, M.M., Schoene, B., Alene, M., Anttila, E.S.C., Tesema, T. Haileab, B., 2019. The lead-up to the Sturtian Snowball Earth: Neoproterozoic chemostratigraphy time-calibrated by the Tambien Group of Ethiopia. GSA Bulletin 132 (5–6), 1119–1149. https://doi.org/10.1130/B35178.1

Patterson, W.P., Walter, L.M., 1994. Depletion of $^{13}$C in seawater $CO_2$ on modern carbonate platforms: Significance for the carbon isotopic record of carbonates. Geology 22 (10), 885–888. https://doi.org/10.1130/0091-7613(1994)022<0885:docisc>2.3.co;2

Prave, A.R., Condon, D.J., Hoffmann, K.H., Tapster, S., Fallick, A.E., 2016.

Duration and nature of the end-Cryogenian (Marinoan) glaciation. Geology 44 (8), 631–634. https://doi.org/10.1130/g38089.1

Prave, A.R., 1999. Two diamictites, two cap carbonates, two $\delta^{13}$C excursions, two rifts: The Neoproterozoic Kingston Peak Formation, Death Valley, California. Geology 27 (4), 339–342. https://doi.org/10.1130/0091-7613(1999)027<0339:TDTCCT>2.3.CO;2

Preiss, W.V., 2000. The Adelaide geosyncline of South Australia and its significance in Neoproterozoic continental reconstruction. Precambrian Research 100 (1–3), 21–63. https://doi.org/http://dx.doi.org/10.1016/S0301-9268(99)00068-6

Rooney, A.D., Macdonald, F.A., Strauss, J.V., Dudás, F.Ö., Hallmann, C., Selby, D., 2014. Re-Os geochronology and coupled Os-Sr isotope constraints on the Sturtian snowball earth. Proceedings of the National Academy of Sciences 111 (1), 51. https://doi.org/10.1073/pnas.1317266110

Rooney, A.D., Strauss, J.V., Brandon, A.D., Macdonald, F.A., 2015. A Cryogenian chronology: Two long-lasting synchronous Neoproterozoic glaciations. Geology 43 (5), 459–462. https://doi.org/10.1130/g36511.1

Rose, C.V., Swanson-Hysell, N.L., Husson, J.M., Poppick, L.N., Cottle, J.M., Schoene, B., Maloof, A.C., 2012. Constraints on the origin and relative timing of the Trezona $\delta^{13}$C anomaly below the end-Cryogenian glaciation. Earth and Planetary Science Letters 319-320, 241–250. https://doi.org/10.1016/j.epsl.2011.12.027

Rose, C.V., Maloof, A.C., Schoene, B., Ewing, R.C., Linnemann, U., Hofmann, M., Cottle, J.M., 2013. The end-Cryogenian glaciation of South Australia. Geoscience Canada; Volume 40, Number 4 (2013). https://doi.org/10.12789/geocanj.2013.40.019

Schlager, W., 1989. Drowning unconformities on carbonate platforms. SEPM Special Publications, 44, 15–25. https://doi.org/10.2110/pec.89.44.0015

Schrag, D.P., Higgins, J.A., Macdonald, F.A., Johnston, D.T., 2013. Authigenic carbonate and the history of the global carbon cycle. Science 339, 540–543 https://doi.org/10.1126/science.1229578

Shao, Y., Farkaš, J., Holmden, C., Mosley, L., Kell-Duivestein, I., Izzo, C., Reis-Santos, P., Tyler, J., Törber, P., Frýda, J., Taylor, H., Haynes, D., Tibby, J., Gillanders, B.M., 2018. Calcium and strontium isotope systematics in the lagoon-estuarine environments of South Australia: Implications for water source mixing, carbonate fluxes and fish migration. Geochimica et Cosmochimica Acta 239, 90–108. https://doi.org/https://doi.org/10.1016/j.gca.2018.07.036

Shirokova, L.S., Mavromatis, V., Bundeleva, I.A., Pokrovsky, O.S., Bénézeth, P., Gérard, E., Pearce, C.R., Oelkers, E.H., 2013. Using Mg isotopes to trace cyanobacterially mediated magnesium carbonate precipitation in alkaline lakes. Aquatic Geochemistry 19 (1), 1–24. https://doi.org/10.1007/s10498-012-9174-3

Singh, U., 1987. Ooids and cements from the late Precambrian of the Flinders

Ranges, South Australia. Journal of Sedimentary Research 57 (1), 117–127. https://doi.org/10.1306/212F8AC1-2B24-11D7-8648000102C1865D

Skulan, J., DePaolo, D. J., Owens, T. L., 1997. Biological control of calcium isotopic abundances in the global calcium cycle. Geochimica et Cosmochimica Acta 61 (12), 2505–2510. https://doi.org/10.1016/S0016-7037(97)00047-1

Swart, P.K., 2008. Global synchronous changes in the carbon isotopic composition of carbonate sediments unrelated to changes in the global carbon cycle. Proceedings of the National Academy of Sciences 105 (37), 13741–13745. https://doi.org/10.1073/pnas.0802841105

Swart, P.K., 2015. The geochemistry of carbonate diagenesis: The past, present and future. Sedimentology 62 (5), 1233–1304. https://doi.org/10.1111/sed.12205

Swart, P.K., Eberli, G., 2005. The nature of the $\delta^{13}$C of periplatform sediments: Implications for stratigraphy and the global carbon cycle. Sedimentary Geology 175 (1–4), 115–129. https://doi.org/http://dx.doi.org/10.1016/j.sedgeo.2004.12.029

Tang, J., Dietzel, M., Böhm, F., Köhler, S.J., Eisenhauer, A., 2008. $Sr^{2+}/Ca^{2+}$ and $^{44}Ca/^{40}Ca$ fractionation during inorganic calcite formation: II. Ca isotopes. Geochimica et Cosmochimica Acta 72 (15), 3733–3745. https://doi.org/http://dx.doi.org/10.1016/j.gca.2008.05.033

Tziperman, E., Halevy, I., Johnston, D.T., Knoll, A.J., Schrag, D.P., 2011.

Biologically induced initiation of Neoproterozoic snowball-Earth events. PNAS 108 (37), 15091–15096.

Vahrenkamp, V.C., Swart, P.K., Ruiz, J., 1991. Episodic dolomitization of late Cenozoic carbonates in the Bahamas; evidence from strontium isotopes. Journal of Sedimentary Research 61 (6), 1002–1014. https://doi.org/10.1306/d4267825-2b26-11d7-8648000102c1865d

Zeebe, R.E., Wolf-Gladrow, D., 2001. $CO_2$ in seawater: equilibrium, kinetics, isotopes. Vol.65. Elsevier Oceanography Series 65.